Hypothalamic dopamine signaling regulates brown fat thermogenesis

Cintia Folgueira[1,2,3], Daniel Beiroa[2,3], Begoña Porteiro[2,3], Manon Duquenne[4], Emma Puighermanal[5], Marcos F. Fondevila[2,3] Silvia Barja-Fernández[1,3], Rosalia Gallego[6], René Hernández-Bautista[2], Cecilia Castelao[1,3], Ana Senra[2], Patricia Seoane[2,3], Noemi Gómez[7], Pablo Aguiar[7], Diana Guallar[2], Miguel Fidalgo[2], Amparo Romero-Pico[2,3], Roger Adan[8], Clemence Blouet[9], Jose Luís Labandeira-García[2,10], Françoise Jeanrenaud[11], Imre Kallo[12], Zsolt Liposits[12], Javier Salvador[3,13], Vincent Prevot[4], Carlos Dieguez[2,3], Miguel Lopez[2,3], Emmanuel Valjent[5], Gema Frühbeck[3,13], Luisa M. Seoane[1,3], Ruben Nogueiras[2,3]

[1] Grupo Fisiopatología Endocrina, Instituto de Investigación Sanitaria de Santiago de Compostela, Complexo. Hospitalario Universitario de Santiago (CHUS/SERGAS), Instituto de Investigación Sanitaria, Santiago de Compostela, Travesía da Choupana s/n, 15706 Santiago de Compostela, Spain

[2] CIMUS, Universidade de Santiago de Compostela-Instituto de Investigación Sanitaria, Santiago de Compostela, 15782, Spain

[3] CIBER Fisiopatología de la Obesidad y Nutrición (CIBERobn), 15706, Spain

[4] Jean-Pierre Aubert Research Center (JPArc), Laboratory of Development and Plasticity of the Neuroendocrine Brain, Inserm UMR-S 1172, Lille, France.

[5] IGF, Inserm, CNRS, Univ. Montpellier, F-34094 Montpellier, France.

[6] Department of Morphological Sciences, School of Medicine, University of Santiago de Compostela, S. Francisco s/n, 15782 Santiago de Compostela (A Coruña), Spain

[7] Molecular Imaging Group, Department of Psychiatry, Radiology and Public Health, Faculty of Medicine Universidade de Santiago de Compostela (USC), Santiago de Compostela 15782 Spain; Molecular Imaging Group. Health Research Institute of Santiago de Compostela (IDIS). Travesía da Choupana s/n Santiago de Compostela. Zip Code: 15706. Spain; Nuclear Medicine Department University Clinical Hospital Santiago de Compostela (SERGAS) (CHUS), Travesía Choupana s/n. Santiago de Compostela 15706 Spain.

[8] Brain Center Rudolf Magnus, Department of Neuroscience and Pharmacology, University Medical Center Utrecht, Universiteitsweg 100, 3584 CG, Utrecht, The Netherlands.

[9] MRC Metabolic Disease Unit. Institute of Metabolic Science. University of Cambridge, UK.

[10] Networking Research Center on Neurodegenerative Diseases, CIBERNED, Madrid, Spain

[11] Laboratory of Metabolism, Division of Endocrinology, Diabetology and Nutrition, Department of Internal Medicine, Faculty of Medicine, University of Geneva, Geneva, Switzerland

[12] Laboratory of Endocrine Neurobiology, Institute of Experimental Medicine, HAS, 1083, Budapest, Hungary

[13] Department of Endocrinology & Nutrition, Clínica Universidad de Navarra & IdiSNA, Pamplona, Spain

Corresponding authors

L. M. Seoane

Grupo Fisiopatología Endocrina, Instituto de Investigación Sanitaria de Santiago de Compostela, Complexo Hospitalario Universitario de Santiago (CHUS/SERGAS), Universidad de Santiago de Compostela (USC), Travesía da Choupana s/n, 15706 Santiago de Compostela, Spain. e-mail: luisamaria.seoane@usc.es

R. Nogueiras

Department of Physiology, Research Centre of Molecular Medicine and Chronic Diseases (CIMUS), Instituto de Investigación Sanitaria de Santiago de Compostela, Universidad de Santiago de Compostela (USC), Santiago de Compostela, Spain. e-mail: ruben.nogueiras@usc.es

Abstract

Dopamine signaling is a crucial part of the brain reward system and can affect feeding behavior. Dopamine receptors are also expressed in the hypothalamus, which is known to control energy metabolism in peripheral tissues. Here we show that pharmacological or chemogenetic stimulation of dopamine receptor 2 (D2R) expressing cells in the lateral hypothalamic area (LHA) and the zona incerta (ZI) decreases body weight and stimulates brown fat activity in rodents in a feeding-independent manner. LHA/ZI D2R stimulation requires an intact sympathetic nervous system and orexin system to exert its action and involves inhibition of PI3K in the LHA/ZI. We further demonstrate that, as early as 3 months after onset of treatment, patients treated with the D2R agonist cabergoline experience an increase in energy expenditure that persists for one year, leading to total body weight and fat loss through a prolactin-independent mechanism. Our results may provide a mechanistic explanation for how clinically used D2R agonists act in the CNS to regulate energy balance.

Introduction

Obesity has reached epidemic prevalence, and much research has focused on homeostatic and hedonic mechanisms underlying overconsumption of food and the regulation of body weight. Dopamine has the ability to modulate food consumption by both reward (hedonic) and hypothalamic (homeostatic) pathways [1]. Among the five dopamine receptors (D1R, D2R, D3R, D4R and D5R), dopamine signaling through D1R [2-4] and D2R regulates food intake [1,5-7]. The increase in central dopaminergic signaling is often associated to the stimulation of feeding, while its decrease has the opposite effect; however in the hypothalamus, the effects on food intake depend on the hypothalamic area targeted [8].

The clinical relevance of the D2R is well characterized and D2R agonists such as bromocriptine and cabergoline, have been widely used for the treatment of prolactinomas. Since 2009 bromocriptine has been also approved in the United States as adjunctive treatment for type 2 diabetes [9], as it improves glucose tolerance and reduces fasting and postprandial plasma glucose levels in diabetic patients [10-12]. In terms of energy homeostasis, obese humans have reduced dopamine levels and/or function [13]. Antipsychotic drugs that block D2R are associated with increased appetite, weight gain and development of diabetes [14,15] and morbidly obese humans have less D2R availability [8]. In addition, human studies have shown a higher prevalence of the *Taq1A* allele for the D2R in obese individuals [16] and genetic variants influencing D2R signaling affect a significant portion of the population [17]. However, the effects of bromocriptine and cabergoline on body weight are contradictory in different studies, albeit most of them non-randomized, reporting either reduction or no significant effects

on body weight [10,18] or no significant effects in body weight in obese or type 2 diabetic patients [19].

In this study, we find that the central stimulation of D2R increases brown adipose tissue (BAT) activity in lean and diet-induced obese rodents in a food intake-independent manner. These central effects are located in GABAergic neurons in the lateral hypothalamic area (LHA) and the neighboring zona incerta (ZI). D2R triggers orexin signaling, which leads to decreased protein kinase A (PKA) activity, increased phosphodiesterase 3B (PDE3B) and reduced ribosomal protein S6 (rpS6) levels. Of note, this thermogenic action depends on the sympathetic nervous system (SNS). Importantly, the clinical relevance of these findings is supported by the fact that patients treated with cabergoline for 12 months showed a significant weight loss, associated with augmented resting energy expenditure, alongside metabolic improvement, through a prolactin-independent mechanism.

Results

Bromocriptine induces negative energy balance and thermogenesis

A single ICV injection of bromocriptine (40 and 80 µg/rat) significantly decreased body weight after 24 hours independently of food or water intake, while a dose of 20 µg/rat did not change body weight (Supplementary Fig. 1a-d). The dose of 80 µg/rat elicited a significant early increase in food intake but after 24 hours the food intake was similar between control and bromocriptine-treated animals. ICV bromocriptine-treated rats (40 µg/rat) showed increased energy expenditure (Supplementary Fig. 1e), BAT

interscapular temperature (Supplementary Fig. 1f) and stimulation of 2-^{18}F-fluoro-2-deoxy-2-glucose (18F-FDG) uptake in BAT analyzed by positron emission tomography-computed tomography (PET-CT) (Supplementary Fig. 1g); while no changes were found in body temperature or respiratory quotient (Supplementary Fig. 1h-i). Consistently, the analysis of histological sections revealed smaller lipid droplets in adipocytes of BAT from bromocriptine-treated rats (Supplementary Fig. 1j), increased BAT UCP1 protein levels (Supplementary Fig. 1k) and increased tolerance to cold exposure (Supplementary Fig. 1l). As expected, the central activation of D2R stimulated locomotor activity at short-term (Supplementary Fig. 1m). To determine the relevance of physical activity on energy expenditure in relation to non-physical activity mechanisms (e.g. resting metabolic rate), we performed correlations and found that energy expenditure and locomotor activity were positively correlated in the dark phase (right panel) but not in the light phase (left panel) (Supplementary Fig. 1n). In addition, we have also analyzed energy expenditure (Kcal/h) during 2 hours of the light phase when animals were less active. During these 2 hours of the light phase, we did not see any difference in energy expenditure between vehicle and bromocriptine treated rats (Supplementary Fig. 1o), suggesting that bromocriptine is not affecting resting metabolic rate. Bromocriptine and cabergoline are used in patients with prolactin□ secreting pituitary adenomas [20], but circulating levels of prolactin in rats treated with bromocriptine ICV remained unchanged when compared to control groups (Supplementary Fig. 1p).

In addition, we injected prolactin ICV in male mice at two different doses (1 and 10 µg/mouse) and after 24 hours (when bromocriptine caused a significant reduction in body weight independent of food intake), we failed to find any statistically significant

effect on body weight and food intake (Supplementary Fig. 2a,b). In keeping, prolactin ICV did not affect BAT interscapular temperature (Supplementary Fig. 2c). Overall, these results indicate that the central administration of prolactin is not altering BAT activity.

To rule out the possibility that centrally injected bromocriptine leaks out of the CNS into the circulation and elicits a response by directly acting at peripheral level, we administered bromocriptine peripherally, using the same dose as the one injected centrally. We were unable to detect changes in food intake, body weight or BAT temperature (Supplementary Fig. 3a-c). Consistent with this, when we injected an adenoviral vector encoding a shRNA against D2R in the BAT [21], the knockdown of D2R specifically in BAT (Supplementary Fig. 3d,e) did not prevent the effects of central bromocriptine on body weight (Supplementary Fig. 3f), food intake (Supplementary Fig. 3g), BAT interscapular temperature (Supplementary Fig. 3h) or BAT UCP-1 levels (Supplementary Fig. 3i). In addition, to assess whether the effect of bromocriptine on BAT was sex-dependent or not, we injected a single ICV injection of bromocriptine (40 µg/rat) in females, and found that identically to males, it significantly decreased body weight and white fat mass after 24 hours, concomitant with increased BAT interscapular temperature, and this effect was again independent of food intake (Supplementary Fig. 4a-e).

We next investigated if the effects of central bromocriptine may be long-lasting. Therefore, we chronically infused bromocriptine (40 µg/rat) during 2 weeks in rats fed a chow diet. We found that cumulative food intake remained unchanged, while body

weight gain was significantly lower in rats treated with bromocriptine (Fig. 1a,b). Histological analyses revealed smaller lipid droplets in BAT of bromocriptine-treated rats, as well as increased protein content of UCP1, FGF21 and PRDM16 (Fig. 1c,d). β-adrenergic receptors represent a key link involved in the regulation of adipose tissue metabolism by the sympathetic nervous system (SNS) [22,23]. To determine whether the central bromocriptine action on BAT was mediated by SNS, we injected the β3 adrenergic receptor specific antagonist SR59230A [24,25] and found that it reversed the effects of central bromocriptine on weight gain (Fig. 1a), BAT lipid content and BAT levels of thermogenic markers (Fig. 1c,d). After that, we assessed the efficacy of the chronic central infusion of bromocriptine in diet-induced obese (DIO) rats. Similarly, to the results obtained in rats fed a chow diet, central bromocriptine reduced body weight gain and adiposity in a feeding independent manner (Fig. 1e-g). Consistently, energy expenditure was also higher (Fig. 1h), with changes neither in respiratory quotient nor locomotor activity (Fig. 1i,j). BAT from bromocriptine-treated DIO rats showed smaller lipid droplets and increased protein content of thermogenic markers (Fig. 1k,l). Moreover, the pharmacological blockade of the β3 adrenergic receptor reversed the effects of central bromocriptine on weight gain, adiposity, energy expenditure, as well as BAT morphology and protein levels of UCP1 (Fig. 1f-l). To finally characterize the relevance of the SNS, triple knockout (TKO) (β1-, β2-, and β3-adrenergic receptors) mice were centrally infused with bromocriptine for 7 days. Bromocriptine did not affect food intake in WT or TKO mice, but significantly decreased body weight gain and white fat mass in WT mice, but not in TKO mice (Fig. 1m-o). In agreement with this, central bromocriptine reduced BAT lipid content and increased BAT UCP1 protein levels in WT but not in TKO mice (Fig. 1p,q).

D2R in the LHA and ZI activates BAT in diet-induced obese (DIO) rats

D2R is widely expressed in the hypothalamus [26]. Therefore, we examined the specific activation of the dopaminergic system in different hypothalamic sites. We found that a single injection of bromocriptine in the LHA and the zona incerta (ZI) (Supplementary Fig. 4f) of rats fed a chow diet decreased body weight and stimulated BAT temperature after 24 hours in a feeding-independent manner (Supplementary Fig. 4g-i). In these animals, circulating levels of prolactin did not change significantly compared to control groups (Supplementary Fig. 4j). When vehicle or bromocriptine were injected in the VMH of rats fed a chow diet (Supplementary Fig. 4k), we found that body weight of vehicle-treated rats decreased after 24 hours, but bromocriptine-treated animals lost more weight and shower higher BAT temperature than controls independent of changes in feeding (Supplementary Fig. 4l-n). Notably, the central injection of bromocriptine in the LHA/ZI (Fig. 2a-e), but not within the VMH (Fig. 2f-h), of DIO rats reduced body weight, increased interscapular temperature, reduced the lipid content in BAT and increased BAT UCP1 protein levels without changing food intake (Fig. 2a-h).

We next used a designer receptor exclusively activated by designer drugs (DREADD) approach to specifically activate D2R neurons in the LHA and the ZI. D2R-Cre mice fed a chow diet were bilaterally injected with AAV-hSyn-DIO-hM3D(Gq)-mCherry in the LHA and the ZI, where its expression was located (Fig. 2i). More specifically, D2R-mCherry neurons occupy the LHA area defined by the fornix/perifornical nucleus, the nigrostriatal bundle, cerebellar peduncle, and the medial tuberal nucleus. After 3 weeks, activation of hM3D(Gq)-mCherry by intraperitoneal (i.p.) injections of clozapine-N-oxide (CNO) (1mg/kg) leads to a decrease in body weight without changes in feeding and water intake (Fig. 2j,k). The decrease in body weight was associated with higher interscapular temperature, energy expenditure and BAT UCP1 protein levels, alongside

226 decreased lipid content in BAT with unaltered body temperature, respiratory quotient,
227 locomotor activity, resting metabolic rate or plasma prolactin levels (Fig. 2l-t). When
228 animals were exposed to 4ºC, the group where D2R were activated in the LHA/ZI
229 showed a cold resistance as demonstrated by an increased capacity to maintain body and
230 BAT temperature (Fig. 2u).

231 Since clozapine metabolite rather than CNO has been shown to mediate the activation
232 of DREADD receptor after i.p injection [27] and clozapine has some affinity with D2R,
233 we also performed an independent experiment using this compound. Similar to CNO,
234 the injection of clozapine decreased body weight and stimulated BAT temperature
235 (Supplementary Fig. 4o,q). We next evaluated the phenotype of mice after
236 chemogenetic activation of D2R neurons at thermoneutrality (30 ºC). At 30 ºC, the
237 activation of D2R neurons in the LHA and ZI resembled the effects found at 23 ºC
238 described above, as the mice presented lower body weight, increased interscapular
239 temperature and energy expenditure without changes in body temperature or locomotor
240 activity (Supplementary Fig. 5a-f). We also performed correlations between energy
241 expenditure and locomotor activity but failed to find any correlation (Supplementary
242 Fig. 5g). In addition, energy expenditure did not change during the 2 hours of the light
243 phase when animals were less active, suggesting that activation of D2R neurons in the
244 LHA/ZI is not affecting resting metabolic rate (Supplementary Fig. 5g).

245

246 To test whether D2R neurons located in other hypothalamic areas were also important
247 for the regulation of BAT activity, we performed chemogenetic activation of D2R
248 neurons in the mediobasal hypothalamus (MBH: ARC + VMH) including the
249 tuberoinfundibular dopamine (TIDA) neurons controlling prolactin secretion from the

anterior pituitary [28], and in the dorsomedial nucleus of hypothalamus (DMH). We found that chemogenetic activation of D2R neurons in the MBH and DMH did not affect body weight, interscapular temperature or white fat mass (Supplementary Fig. 6).

The effect of bromocriptine on BAT is dependent on D2R in the LHA/ZI

We stereotaxically delivered an adenoviral vector encoding a shRNA against D2R in the LHA/ZI in rats fed a chow diet. Infection efficiency in the LHA and ZI was assessed by expression of GFP and decreased levels of D2R (Fig. 3a,b). Although the selected titer of the adenoviral vector inhibiting D2R in the LHA/ZI did not affect either body weight or food intake, it attenuated bromocriptine–induced weight loss (Fig. 3c,d). In agreement with these results, the effect of bromocriptine on adiposity, BAT temperature, lipid content and UCP1 levels was absent when D2R was inhibited in the LHA/ZI (Fig. 3e-h). Furthermore, rats receiving bromocriptine in the LHA/ZI displayed a significant increase in c-FOS staining in the raphe pallidus (RPa) and the inferior olive (IO), which was indicative of higher neuronal activation (Fig. 3i).

However, the knockdown of D2R in the VMH (Supplementary Fig. 7a) of rats fed a chow diet did not ameliorate bromocriptine–induced weight loss, adiposity or interscapular temperature (Supplementary Fig. 7b-e). To further confirm the relevance of the LHA/ZI in the actions of bromocriptine, we performed another experiment injecting in the LHA/ZI the adenoviral vector inhibiting D2R (Supplementary figure 7f) and two weeks later, mice were treated with systemic bromocriptine at a dose higher than the one administered ICV. This intraperitoneal dose (5 mg/kg) decreased body weight, WAT mass and activated BAT temperature and UCP1 protein levels

(Supplementary Fig. 7g-k). However, these effects were completely abolished when the D2R was inhibited in the LHA/ZI (Supplementary Fig. 7g-k).

D2R action in GABAergic neurons requires orexin to modulate BAT

The LHA and the ZI are mainly composed by multiple neuronal populations expressing different neuropeptides and neurotransmitters. To identify which neuronal populations were expressing D2R, we used a D2R-cre:ribotag mouse line [29]. HA immunoreactivity allowing the identification of D2R-positive cells was detected in GABAergic and glutamatergic neurons in the LHA and the ZI, but not in cells expressing MCH or orexin (Fig. 3j). To know the functional relevance of GABAergic and glutamatergic neurons in the actions of D2R, we over-expressed D2R in these neuronal populations injecting a viral vector (Ad-hSyn-DIO-D2R) in the LHA/ZI of Vglut2- ires-cre and Vgat-ires-cre mice. Fluorescent activated cell sorting (FACS) demonstrated that the virus targeted 198.2 ± 10.2 cells per animal in the LHA/ZI and confirmed D2R expression in GABAergic and glutamatergic neurons (Fig. 4g). The gating strategy for FACS is detailed in Supplementary fig 8. We found that over-expression of D2R in GABAergic (Fig. 4f-k), but not glutamatergic cells of the LHA/ZI (Fig. 4a-e), reduced body weight and increased interscapular temperature and UCP1 protein levels independent of food intake. In line with this, the inhibition of D2R in GABAergic neurons of the LHA/ZI using a viral vector expressing a shRNA against D2R (Ad-hSyn-DIO-shD2R) increased body weight and decreased interscapular temperature when compared to control mice (Fig. 4l-o).

Since GABA regulates the activity of different neuronal populations in the LHA, we next tested whether the effects of the hypothalamic dopamine system required orexin or

MCH, two neuropeptides known to be involved in thermoregulation [30,31]. We found that bromocriptine administered ICV increased orexin, but not MCH, mRNA levels in the LHA (Supplementary Fig. 9a). Similarly, bromocriptine directly injected in the LHA/ZI augmented orexin protein levels (Supplementary Fig. 9b), the knockdown of D2R in the LHA/ZI prevented bromocriptine-induced orexin protein levels (Supplementary Fig. 9c), and the chemogenetic activation of D2R in LHA/ZI stimulated orexin levels (Supplementary Fig. 9d). The specific isolation of the LHA/ZI was corroborated by measuring protein levels of orexin and MCH, which are specifically located in the LHA and were not detected in the VMH (Supplementary Fig. 9e). Although there are no specific markers for the ZI, the isolated micropunches included the LHA and also ZI, because due to their neighboring localization and the lack of specific markers, it is virtually impossible to separate it from the LHA. Moreover, the specificity of the antibodies for D2R, orexin and MCH was tested in D2R null mice, orexin null mice and rats injected with an MCH antisense oligonucleotide respectively (Supplementary Fig. 10a).

To investigate the mechanistic link between LHA D2R and the orexin system, we next assessed the effects of central bromocriptine in mice lacking orexin. We found that while in WT mice bromocriptine decreased body weight in a food-independent manner, increased interscapular temperature, decreased lipid content in BAT and up-regulated BAT UCP-1 protein levels, it was unable to exert these actions in orexin-deficient mice (Fig. 4p-t).

To further characterize the role of orexin as a mediator of dopamine actions, we performed chemogenetic stimulation of D2R neurons in the LHA/ZI and concomitant treatment with the orexin receptor 1 antagonist SB-334867 [32]. Our findings demonstrated that the effects of D2R activation in the LHA/ZI on body weight,

interscapular temperature, BAT lipid content and UCP1 levels were completely blocked when SB-334867 was injected ICV (Fig. 4u-x).

Phosphodiesterase 3B and protein kinase A mediate the actions of bromocriptine

Protein kinase A (PKA) signaling has been related to non-metabolic dopamine D2R actions in some extra-hypothalamic areas [33,34]. Herein, we measured phosphorylated cAMP response element-binding protein (pCREB) as a marker of PKA activity [35]. We found that both bromocriptine administered either ICV or in the LHA/ZI (Fig. 5a,b) and chemogenetic activation of D2R in the LHA/ZI (Fig. 5c) decreased pCREB protein levels, an effect that was blunted by the injection of the orexin receptor 1 antagonist (Fig. 5c). This decrease in pCREB levels was also detected after the injection of orexin A, an effect blocked by the orexin receptor 1 antagonist (Fig. 5d). Thus, these data indicate that both bromocriptine and orexin modulate PKA activity.

Central injection of the specific PKA activator Sp-cAMPS (90 ng/rat) [35,36], abolished the effects of bromocriptine on body weight, white mass, BAT interscapular temperature, lipid content and UCP1 protein levels in a feeding-independent manner after 24h (Fig. 5e-j). Furthermore, the administration of the PKA inhibitor H-89 (62 ng/rat) [35,36] in the LHA/ZI recapitulated the effects of bromocriptine, since it decreased body weight, white mass and BAT lipid content and stimulated BAT interscapular temperature and UCP1 protein levels (Fig. 5k-p) independent of food intake.

Phosphodiesterases (PDEs) are enzymes that break a phosphodiester bond and are classified in different families. PDE3 is highly sensitive to inhibition of cAMP hydrolysis by cGMP, and there are 2 PDE3 isoforms which are encoded by different genes (PDE3A and PDE3B) [37]. Hypothalamic PDE3B was found to play a relevant role regulating the action of leptin on feeding [38] and insulin [39]. PDE3B is also related to hypothalamic leptin signaling during the development of diet-induced obesity [40]. We measured protein levels of PDE3B in the LHA/ZI of mice and found that after the chemogenetic stimulation of D2R in this hypothalamic area, PDE3B levels were increased compared to control mice (Fig. 5q). Then, we injected ICV the PDE3 inhibitor cilostamide at a reported dose (10 μg/mouse) [39] that did not affect body weight or food intake (Fig. 5r,s). However, this dose of cilostamide blocked the effects of chemogenetic activation of D2R on body weight and interscapular temperature (Fig. 5t-v). Finally, we injected cilostamide ICV in mice where D2R was over-expressed in GABA neurons injecting the Ad-hSyn-DIO-D2R in the LHA/ZI of Vgat-ires-cre mice; our data showed that cilostamide ameliorated the suppression of body weight and stimulation of BAT activity and increased energy expenditure induced by D2R overexpression in GABA neurons (Fig. 5w-z). Overall, these results indicate that PDE3B mediates the central effects of the hypothalamic dopamine system within LHA/ZI on body weight and BAT activity.

rpS6 in the LHA/ZI modulates the actions of bromocriptine

PKA has been identified to regulate ribosomal protein S6 (rpS6) [41,42]. Thereby, we investigated the possibility that rpS6 was mediating the actions of bromocriptine on energy balance. Phosphorylated levels of rpS6 (P-rpS6) were significantly decreased

after the injection of bromocriptine ICV (Fig. 6a,b) or in the LHA/ZI (Fig. 6c), an effect that was blunted when D2R was knocked down specifically in the LHA/ZI (Fig. 6d) and when bromocriptine was injected in orexin-deficient mice (Fig. 6e). The chemogenetic activation of D2R in the LHA/ZI also resulted in lower P-rpS6 protein levels, and this effect was prevented by the antagonism of orexin receptor 1 (Fig. 6f). In line with this, orexin, which also down-regulates P-rpS6 levels failed to do that when the orexin receptor 1 antagonist was given (Fig. 6g). These results suggest that both D2R and orexin signaling were important for the modulation of P-rpS6. Importantly, the effects of bromocriptine on P-rpS6 were specific, because when we measured hypothalamic protein levels of multiple molecules known to have important effects on energy homeostasis such as phosphorylated c-Jun N-terminal kinase (pJNK), JNK, phosphorylated protein kinase B (pAKT), AKT or mammalian target of rapamycin (mTOR), they remained unaltered after bromocriptine treatment (Supplementary Fig. 10b). In addition, we found that the administration of H-89 in the LHA/ZI decreased P-rpS6 levels (Fig. 6h), and that the activation of PKA by Sp-cAMPS blunted bromocriptine-induced rpS6 inhibition (Fig. 6i).

Given that rpS6 was regulated by bromocriptine/orexin/PKA, we next performed a functional study using an adenovirus encoding a constitutive active form of S6K (CA-S6K-Ad) [43] in the LHA/ZI. We confirmed the efficiency of the viral vector by detecting increased P-rpS6 protein levels 8 days after the stereotaxic administration of CA-S6K-Ad (Fig. 6j). Although the dose of the adenoviral vector activating S6K in the LHA/ZI did not affect food intake or body weight, it attenuated bromocriptine–induced weight loss (Fig. 6k,l), the increase in interscapular temperature (Fig. 6m), the reduction of lipid content in BAT (Fig. 6n) and the up-regulation of BAT UCP1 (Fig. 6o). To note,

the activation of S6K did not modify the bromocriptine-induced orexin levels in the LHA/ZI, confirming that rpS6 is downstream orexin (Ad Null LHA/ZI+ Vehicle ICV: 100± 9.1, Ad Null LHA/ZI + BC (40ug/rat)ICV: 136.7±9.6, Ad S6K1 LHA/ZI+ Vehicle ICV:104,0± 8.9, Ad S6K1 LHA/ZI+ BC (40ug/rat) ICV: 126,2±6.8).

Dopamine agonism decreases body weight in hyperprolactinemic patients

In the retrospective study after one year of cabergoline treatment instauration with 0.5 mg twice weekly all patients normalized the hyperprolactinemia irrespective of sex. Side effects were infrequent and very mild (nausea and postural hypotension) and no patient was withdrawn from the treatment for this reason. A statistically significant decrease in body weight and BMI were observed (Table 1 and Fig. 7a). Noteworthy, a huge inter-individual variability in weight loss was evident (Fig. 7a). Of interest, after 12 months of cabergoline treatment a statistical improvement in glucose metabolism as evidenced by decreases in glucose and insulin concentrations as well as in the insulin resistance HOMA-IR index was observed. The same was true for the lipid profile with significant reductions in the levels of triglycerides, total and LDL cholesterol. No sex differences were observed as regards both the anthropometric and metabolic changes.

Dopamine agonism increases energy expenditure in hyperprolactinemic patients

To gain more insight into the potential impact of dopamine agonism on body weight, body composition, resting energy expenditure and metabolic changes were analysed in a prospective study in patients affected by hyperprolactinemia. As observed in the retrospective study one year after cabergoline treatment instauration with 0.5 mg twice weekly all patients normalized the hyperprolactinemia irrespective of sex. Side effects

were again infrequent and very mild (nausea, postural hypotension and dizziness) with no patient withdrawing from the treatment. In this case, the statistically significant reduction in body weight and BMI was already observed after 3 months of cabergoline treatment start (Fig. 7b) and persisted after 12 months (Table 1). Again, patients exhibited a huge inter-individual variability in weight loss both after 3 and 12 months following cabergoline treatment irrespective of the weight category (Fig. 7b). The magnitude of weight loss was greater after 3 as compared to 12 months. Noteworthy, following cabergoline treatment body composition analysis showed a significant decrease of both total and visceral adiposity as evidenced by reduction of body fat percentage and waist circumference, respectively (Table 1). In line with the anthropometric changes observed, a statistically significant increase in REE was documented expressed in absolute terms or adjusted by either total body weight or fat-free mass. Importantly, patients showed the REE predicted from the Harris Benedict equation before starting the cabergoline treatment, however after 3 months of treatment the REE was significantly higher than the theoretical REE (Fig. 7c); and there was a positive correlation between the REE adjusted per body weight after cabergoline treatment and weight loss (Fig. 7d). Cabergoline treatment was followed by a significant improvement in glucose metabolism as evidenced by decreases in glucose and insulin concentrations as well as in the insulin resistance HOMA-IR index which was already evident after 3 months. Triglyceride concentrations experimented also a significant decrease after 3 and 12 months of cabergoline start, although in this case no changes in total, LDL and HDL cholesterol levels were observed. As in the retrospective study, no significant differences in the anthropometric, REE and metabolic effects between men and women took place.

Discussion

Our findings indicate that the brain dopamine system directly activates BAT thermogenesis in a feeding-independent manner. More specifically, these actions are mediated by the stimulation of D2R in GABAergic neurons located within the LHA and the ZI, which activates the SNS and ultimately leads to the increase of UCP1, BAT temperature and energy expenditure. This process is mediated by the up-regulation of orexin and PDE3B, which in turn decreases cAMP and the activity of PKA and rpS6. To our knowledge, these findings are the first to provide information about the brain site and mechanisms by which fat mass decreases in response to a stimulation of CNS D2R activity, independently of anorexigenic actions. We also observed that patients treated with cabergoline, a D2R agonist, for 12 months showed a reduction in BMI and body fat together with an increase in resting energy expenditure and an improvement in glucose and lipid metabolism.

The mechanisms by which central dopamine affects body weight are widely assumed to be related to food intake and reward [17,44]. Within the hypothalamus, dopamine levels in the LHA immediately increase in response to feeding and normalize after meal consumption [45-47], and injection of D2R antagonists in the LHA reverses amphetamine-induced anorexia [48,49]. However, dopamine levels in the VMH decrease after feeding and increase during fasting [50] and dopamine injection in this area increased meal size while decreasing meal number [51]. In line with this, tyrosine hydroxylase neurons of the ARC excited AgRP neurons and inhibited POMC neurons, suggesting that dopamine has an orexigenic action in this hypothalamic site [52]. More recently, one report has shown that activation of striatal D2R reduced BAT thermogenesis and energy expenditure, and accelerated obesity despite reduced eating [53]. That study supports the idea that the dopamine system may exert different actions depending on the

hypothalamic site. Nevertheless, some report showed that although chronic obesogenic diets reduce striatal D2R function, striatal D2R down-regulation does not lead to obesity [54,55], suggesting that changes in striatal D2R expression could be a consequence rather than the cause of obesity.

In addition to the well-known effects on food intake, the hypothalamic areas where D2R is highly expressed, are also important centers for the control of BAT activity [56]. Therefore, we hypothesized that D2R stimulation at this level could trigger BAT thermogenesis. We found that chronic central infusion of bromocriptine increases BAT activity and ameliorates diet-induced obesity, independently of feeding. These effects are regulated by the SNS, since its pharmacological or genetic disruption blunts bromocriptine-induced effects on BAT. The hypothalamic area responsible for the effects of bromocriptine resides in the LHA and the ZI, since pharmacological and chemogenetic stimulation of D2R in these areas reduces HFD-induced adiposity due to increased BAT activity and higher energy expenditure. The chemogenetic stimulation of D2R neurons in the LHA/ZI, but not in the VMH or DMH, also stimulated BAT activity and decreased adiposity in conditions of thermoneutrality. Supporting these data, the loss-of-function of D2R by shRNA in the LHA/ZI was enough to block the actions of central and peripheral bromocriptine on BAT function. Therefore, these results indicate that the site of action of the dopamine system to regulate BAT activity occurs specifically in the LHA/ZI but not in other hypothalamic regions.

In line with this, even though dopamine receptors have been detected in brown adipocytes and dopamine stimulates thermogenesis in these cells [57], when we inhibited

D2R in BAT, central bromocriptine was still able to decrease body weight and increase BAT temperature. Overall, our *in vivo* results indicate that the thermogenic action of bromocriptine requires the presence of D2R in the LHA/ZI, while D2Rs located in BAT are not necessary. Previous reports have suggested that the effects on food intake occur in the ARC and VMH and our present findings indicate that chemogenetic activation of D2R in the MBH, which includes ARC and VMH, or in the DMH, does not affect BAT thermogenesis while D2R neurons in the LHA and ZI regulate BAT and increase energy expenditure. Therefore, the effects of dopamine on food intake from those on energy expenditure are dissociated since dopamine requires the ARC to regulate food intake [52] and the present study indicates that dopamine actions in the LHA and ZI controls BAT activity and energy expenditure.

The LHA and ZI are heterogeneous brain areas containing numerous genetically distinct cell populations that use a plethora of signaling mechanisms. Our findings indicate that D2R is located in both glutamatergic and GABAergic cells, but only genetic manipulation of D2R only in GABAergic neurons exert marked effects on body weight. This is of relevance because both GABA neurons and dopamine modulate orexin activity [58,59]. A key role of orexin is related to energy expenditure via the regulation of thermogenesis [31,32,60,61]. However, despite these data it was totally unknown whether the interaction with central dopamine system could play a significant role in energy homeostasis. To address that possibility, we investigated whether the central thermogenic effect of bromocriptine was associated with orexin function. Our findings indicate that central stimulation of D2R increased orexin expression and that bromocriptine failed to activate BAT thermogenesis in orexin-deficient mice. In agreement with this, the effect of the chemogenetic stimulation of D2R neurons in the

517 LHA/ZI was blunted after the central blockade of the OX1R. Thus, our results indicate
518 that orexin mediates the thermogenic effects of brain D2R stimulation.

519

520 Dopamine has been related with cAMP-dependent signaling. More precisely, the
521 activation of D2R inhibits [62], while the D2R antagonist haloperidol promotes the
522 stimulation of cAMP-dependent PKA and increased the phosphorylation of rpS6 in
523 neurons of the striatum [42]. Moreover, phosphodiesterase (PDE), and more precisely
524 PDE3B is highly sensitive to inhibition of cAMP hydrolysis by cGMP [37]. Hypothalamic
525 PDE3B, plays a relevant role regulating the action of leptin [38] and insulin [39]. Our results
526 indicate that PDE3B mediates the central effects of the dopamine system on body
527 weight and BAT activity. Thus, our current model is that high levels of PDE3B degrade
528 cAMP and these low levels of cAMP subsequently determine the low activity of PKA.
529 Hypothalamic PKA [35,63] and rpS6 [43] have been reported to play a relevant role in the
530 control of energy balance, but their role within the LHA is still unexplored.
531 Furthermore, PKA has been identified as a regulator of rpS6 in neuronal cells [42].
532 Therefore, we hypothesized that bromocriptine might be using this pathway in the LHA
533 to exert its actions on BAT. Our findings demonstrate that both pharmacological and
534 chemogenetic activation of D2R decreased PKA activity, measured by the surrogate
535 marker pCREB. Accordingly, the direct injection of the PKA inhibitor named H-89 in
536 the LHA/ZI stimulated BAT activity and decreased body weight, and the activation of
537 PKA by Sp-cAMPS totally blunted bromocriptine effects on weight loss, BAT
538 temperature and UCP1 expression. Overall, these results indicate that bromocriptine-
539 mediated actions on BAT activity are mediated by PKA-catalyzed phosphorylation of
540 rpS6. In line with our findings, previous studies showed that the inactivation of central
541 PKA, achieved by the disruption of several of its subunits causes resistance to diet-

induced obesity [64,65]. However, to our knowledge, this is the first study addressing the relevant role of PKA in the LHA/ZI.

In line with the findings made in rodents, dopamine agonism in both our retrospective and prospective studies of hyperprolactinemic patients decreased body weight and improved glucose and lipid metabolism. The weight loss was accompanied by a reduction in both total body fat and visceral adiposity. Interestingly, dopamine agonism achieved by cabergoline treatment in hyperprolactinemic patients resulted in an increase in REE which is consistent with the bromocriptine-induced effects on BAT observed in rodents. Moreover, in patients treated with cabergoline, the weight loss is positively correlated to REE. Our observations are in agreement with previous studies of bromocriptine or cabergoline treated patients [66-68]. Noteworthy, while cabergoline decreases body weight in both lean and overweighed patients irrespective of BMI a clear variability in this response is observed, and patients with higher BMIs are in a position of losing more excess weight. Our preclinical studies indicate that prolactin is not mediating the effects of bromocriptine nor chemogenetic manipulation of neuroendocrine TIDA neurons on body weight and BAT activity. In line with this, in human studies it is unlikely that weight loss is secondary to normalization of prolactin, because all the patients with prolactinomas treated with cabergoline showed a normalization in prolactin levels. Despite that prolactin levels are normalized in all these patients treated with cabergoline, they showed changes in body weight. Therefore, there is no correlation between circulating prolactin levels and body weight.

In summary, this study reveals that the activation of D2R in GABA neurons within the LHA and ZI stimulates orexin and PDE3B, which lowers cAMP levels and inhibits a PKA-rpS6. This increases SNS tone, upregulates BAT thermogenesis, and increases energy expenditure, leading to weight loss. In line with this, patients undergoing treatment with the dopamine agonist cabergoline experimented an increase in energy expenditure, leading to total body weight and fat loss. Therefore, this study provides mechanistic insight into the mechanisms taking place at the CNS by which bromocriptine/cabergoline exert their beneficial effects on energy balance and metabolic homeostasis in the clinical setting.

Material and Methods

Animals and diets

Male and female Sprague-Dawley rats (200-250 g); WT and triple b-adrenoreceptor (AR) knockout (TKO) male mice (weight 20–25 g, age 8–10 weeks old) [69,70]; WT and orexin knockout male mice (null *Ox*/*Hcrt* mice, *orexin*/*hypocretin*; *B6.129S6-Hcrttm1Ywa*/*J*, The Jackson Laboratory) (weight 25–30 g, age 10–12 weeks old) [32], WT and Drd2-cre male mice (C57BL/6J, weight 20–25 g, age 8–10 weeks old) [71], Drd2-cre:riboatg mice (weight 25-30 g, age 8-10 weeks old) [29], vgat-ires-cre knock-in (C57BL/6J) and vglut2-ires-cre knock-in (C57BL/6J) from Jackson Laboratory (weight 20-25g, age 8-10 weeks old) were used for the experiments and littermates controls were used in each experiment (Reporting Summary). Except Drd2-cre:ribotag mice, all animals were housed in individual cages under controlled conditions of illumination (12 h light/dark cycle), temperature and humidity. The animals were allowed free access to water and a standard laboratory diet (CD) (Scientific Animal Food & Engineering,

proteins 16%, carbohydrates 60% and fat 3%) or high fat diet (HFD) (Research Diets 12492; 60% of calories from fat, 5.24 Kcal/g; Research Diets, New Brunswick, NJ) for 12 weeks. Food intake and body weight were measured daily during the experimental phase in all experiments. 4 to 12 animals per group were used. The animals were euthanatized, and all the tissues were removed rapidly, frozen immediately on dry ice, and kept at -80ºC until analysis. All experiments and procedures involved in this study were reviewed and approved by the Ethics Committee of the University of Santiago de Compostela, in accordance with European Union normative for the use of experimental animals.

Body composition and indirect calorimetry

Body composition (white fat mass) was measured using a nuclear magnetic resonance system (Whole Body Composition Analyser; EchoMRI, Houston,TX). Measurements were performed before surgery and on the last day of the treatment. Energy expenditure, respiratory quotient (RQ) and locomotor activity were assessed using a calorimetry system (LabMaster; TSE Systems) [24,72].

Temperature measurements, thermal imaging, cold exposure and thermoneutrality

Interscapular temperature was assessed and was visualized using a high-resolution infrared camera (E60bx: Compact-Infrared-Thermal-Imaging-Camera; FLIR; West Malling, Kent, UK) and analyzed with a FLIR-Tools specific software package [73]. Body temperature was recorded with a rectal probe connected to a digital thermometer (BAT-12 Microprobe-Thermometer; Physitemp; NJ, USA). After the acute injection of

613 bromocriptine, rats were placed for 6 h in a special room with a stable temperature of
614 4ºC [74]. D2r-cre mice were moved to a thermoneutral environment (30ºC with relative
615 humidity of 45-52%) in order to eliminate the extra-metabolism needed to defend the
616 body temperature at lower temperatures [75].
617

618 *Intracerebroventricular treatments*

619 Animals were anesthetized by an intraperitoneal injection of a mixture of ketamine-
620 xylazine (ketamine 100 mg/kg rat body weight + xylazine 15 mg/kg rat body weight;
621 ketamine 8 mg/kg mouse body weight + xylazine 3 mg/kg mouse body weight).
622 Intracerebroventricular (ICV) cannulae aimed at the lateral ventricle were
623 stereotaxically implanted in rats using the following coordinates: 1.3 mm posterior to
624 bregma, 1.9 mm lateral to the midsagittal suture, and a depth of 3.5 mm; and in mice:
625 0.6 mm posterior to bregma, 1.2 mm lateral to the midsagittal suture, and a depth of 2
626 mm [72,76]. Animals received vehicle (DMSO 100 mM) or bromocriptine mesylate (20, 40
627 or 80 µg/animal; Tocris, St Louis, MO, USA). In other experiments, the orexin receptor
628 1 inhibitor (SB-334867; 4 µg/mouse, Tocris, St Louis, MO, USA), orexin (10
629 µg/mouse, Bachem, Bubendorf, Switzerland) [32,77], the specific PKA activator Sp-
630 cAMPS (90 ng/rat dose; Tocris, St Louis, MO, USA) [35,36], prolactin (1 or 10 µg/mouse,
631 San Diego, CA, USA) or cilostamide (10 µg/mouse, AlfaAesar, Massachusetts, USA) [39]
632 were also administered ICV. For chronic experiments, a catheter tube was connected
633 from the brain infusion cannulae to an osmotic minipump flow moderator (model 2002
634 for a 14-days period for rats and model 1007D for a 7-days period for mice; Alzet
635 Osmotic Pumps, Durect, Cupertino, CA). These pumps had a flow rate of 0.5 µl/hour
636 during the days of treatment. The minipump was inserted in a subcutaneous pocket on
637 the dorsal surface of the animal that we created using blunt dissection and the incision

was closed with surgical sutures. After surgery, animals were kept warm until they fully recovered.

Peripheral treatments

For peripheral treatments, rats received an intraperitoneal administration of bromocriptine (40 µg/rat) and mice (5 mg/kg). Mice received an intraperitoneal administration of clozapine-N-oxide (CNO; 1 mg/kg, Sigma-Aldrich; St.Louis, MO) and clozapine (1mg/kg, Sigma-Aldrich; St. Louis, MO) [27]. Pharmacological inactivation of β3-adrenoreceptor was performed by subcutaneous administration of the specific antagonist SR59230A (Tocris, St Louis, MO, USA) at a dose of 3 mg/kg [24].

Stereotaxic microinjections in specific hypothalamic nuclei

Rats were placed in a stereotaxic frame (David Kopf Instruments, Tujunga, CA, USA) under ketamine-xylazine anesthetics. Bromocriptine (40 µg/rat) and the specific PKA inhibitor H-89 (62 ng/rat; Sigma Chemical, USA) were injected stereotaxically with a 25-gauge needle (Hamilton, Reno, NV, USA) connected to a 1 µl syringe. We targeted the lateral hypothalamus area and zona incerta (LHA/ZI) and the ventromedial hypothalamus area (VMH) [72]. The coordinates used to reach the LHA/ZI in rats were (anterior to the bregma (AP), -2.85 mm; lateral to the sagittal suture (L), ±2 mm; and ventral from the surface of the skull (DV), -8.1 mm) and to reach the VMH were (AP, -2.85 mm; L, ±0.6 mm; DV, -10 mm). The coordinates used to reach the LHA/ZI in mice were (AP, -1.3 mm; L, ±1.1 mm; DV, -5.2 mm), to reach the MBH were (AP-1.5 mm; L, ±0.2 mm; DV, -6 mm) and to reach the DMH were (AP-1.9 mm; L, ±0.3 mm; DV, -5

mm). The incision was closed with sutures and acetylsalicylic acid (Bayer, Leverkusen, Germany) 150 mg/kg was injected intraperitoneally after surgery as a painkiller.

Stereotaxic microinjection of adenoviral expression vectors

Adenoviral vectors D2R knockdown (3.5 x 10^{10} PFU/ml) or the vector controls (3.5 x 10^{10} PFU/ml) [78] and adenoviral vectors containing the constitutively active form of S6K1 (4.77 x 10^{10} PFU/ml) or null controls (1.8 × 10^{10} PFU/ml) [43] were used. To modify the expression of D2R specifically in vgat and vglut2 neurons, we injected Ad-hSyn-DIO-D2R-EGFP (1.0 x 10^{10} PFU/ml), Ad-hSyn-DIO-shD2R-EGFP (1.0 x 10^{10} PFU/ml) and Ad-hSyn-DIO-EGFP (1.0 x 10^{10} PFU/ml) (Vector Builder) under cell specific cre promoters. These viral vectors were injected in the hypothalamic nuclei as described in the previous section.

FACS sorting and Quantitative RT-PCR analyses

Viral infection was confirmed using FACS. The tuberal region of the hypothalamus of Vgat-cre + Ad-EGFP LHA/ZI mice were microdissected and enzymativcally dissociated using Papain Dissociation System (Worthington, Lakewood, NJ) to obtain single cell suspensions [79]. FACS was performed using an EPICS ALTRA Cell Sorter Cytometer device (BD Bioscience). The sort decision was based on measurements of EGFP fluorescence (excitation: 488 nm; 50 mW; detection: EGFP bandpass 530/30 nm, autofluorescence bandpass 695/40 nm) by comparing cell suspensions from non-infected brain sites (i.e., cortex) and infected brain sites (i.e., the hypothalamus), as indicated in Figure 4g. For each animal 150 to 400 EGFP-positive cells were sorted

684 directly into 10 µl of extraction buffer: 0.1% Triton X100 (Sigma-Aldrich) and 0.4 unit/
685 µl RNaseOUT™ (Life technologies). RNAs obtained from FACS-sorted EGFP-
686 negative and positive cells were reversed transcribed using SuperScript® III Reverse
687 Transcriptase (Life Technologies) and a linear preamplification step was performed
688 using the TaqMan® PreAmp Master Mix Kit Protocol (P/N 4366128, Applied
689 Biosystems). Real-time PCR was carried out on Applied Biosystems 7900HT Fast Real-
690 Time PCR system using exon-boundary-specific TaqMan® Gene Expression Assays
691 (Applied Biosystem): VGat (*Slc32a1*-Mm00494138_m1), Dopamine receptor 2 (*Drd2*-
692 Mm00438545_m1) and VGlut2 (*Slc17a6*-Mm00499876_m1). Control housekeeping
693 genes: R18S (*r18S*-Mm03928990_g1) and Actin (*Actb*-Mm00607939_s1).

694

695 *Designer Receptors Exclusively Activated by Designer Drugs*

696 The hM3Dq coding sequences were cloned into a mCherry vector upstream of the
697 mCherry sequence to generate C-terminal mCherry fusion proteins (Addgene,
698 Cambridge, USA). The hM3Dq-mCherry coding sequence was amplified by PCR, and
699 the amplicons and a cre-inducible AAV vector with a human *Synapsin 1* promoter was
700 packaged in serotype 8: $7.53X10^{12}$ PFU/ml genome copies per ml and was prepared and
701 tittered at the Universidad Autónoma de Barcelona (Barcelona, Spain). Ketamine-
702 xylazine anesthesized male *D2-cre* mice [80] were placed in a stereotaxic frame (David
703 Kopf Instruments). The CRE-dependent AAVs were injected bilaterally into the
704 LHA/ZI of all mice. The viral particles (1 µl, $7.53X10^{09}$ PFU/ml) were infused over 15
705 minutes. Three weeks after the injection of the AAVs, mice received CNO (1 mg/kg of
706 body weight) or vehicle- i.p. injection.

707

Adenoviral injection in the BAT of mice

Adenoviral vectors for knocking down D2R (1.0 x 10^9 PFU/ml) or the vector controls (1.0 x 10^9 PFU/ml) were injected in a volume of 50 µl bilaterally into the BAT in mice under ketamine-xylazine anesthetics [21].

PET imaging system

Whole-body micro PET/CT images were acquired with the Albira PET/CT Preclinical Imaging System (Bruker Biosping; Woodbidge, CT, USA) and the experimental procedure with rats were performed in the same conditions. BAT area was delineated by using image tools implemented the AMIDE Software (http://amide.sourceforge.net/) to generate a three-dimensional spherical volume of interest with radius of 6mm and centered on the BAT area. Mean standardized uptake values (SUV) were computed. The PET-CT analysis was performed in the Molecular Imaging Unit of the Department of Nuclear Medicine of University of Santiago de Compostela.

Dissection of brain areas

The brains were removed and immediately frozen and stored at −80°C until further processing. Then, the brain was placed in a brain matrix with a ventral surface on top under a dissecting microscope. The LHA/ZI were removed from the whole hypothalamus by cutting between the rostral and caudal limits of the median eminence parallel to the base of the hypothalamus and 1 mm to each lateral side of the median eminence. The depth of each section isolated was around 1 mm thick in mice and 3mm thick in rats brain [81,25].

Western Blot analysis

Tissues were homogenized using a TissueLyser II (Qiagen, Tokyo, Japan) in cold RIPA buffer (containing 200 mMTris/HCl (pH 7.4), 130 mM NaCl,10%(v/v) glycerol, 0.1%(v/v) SDS, 1%(v/v) Triton X-100, 10 mM MgCl2) with anti-proteases and anti-phosphatases (Sigma-Aldrich;St.Louis, MO). The tissue lysates were centrifuged for 30 minutes at 18000 g in a microfuge at 4ºC. Brown adipose tissue (BAT), muscle, cortex, VMH and LHA total protein lysates were subjected to sodium–dodecyl sulfate-polyacrylamide gels (SDS–PAGE), then electrotransferred on a PVDF membrane and probed successively with the following antibodies: UCP1, FGF21, PRDM16, D2R, Myostatin (Abcam, Cambridge, UK); PGC1α, JNK, MCH (Santa Cruz Biotechnology, CA, USA); pAKT (Ser473), AKT, phospho-S6 ribosomal protein, S6 ribosomal protein, phospho-SAPK/JNK(Thr183/Tyr185, phospho-CREB (Ser133) (Cell Signaling, USA); GAPDH (Merck Millipore, Darmstadt, Germany); mTOR, β-actin, α-tubulin (Sigma-Aldrich, St. Louis,MO); Myogenin (DSHB, Iowa, USA); Orexin A (Bioss Antibodies, Massachusetts, USA); PDE3B (Invitrogen, CA, USA) after incubating the membranes with 5% BSA blocking buffer. For protein detection we used horseradish-peroxidase-conjugated secondary antibodies (Dako Denmark, Glostrup, Denmark). Specific antigen-antibody bindings were visualized using chemiluminescence method according to the manufacturer´s instructions (Pierce ECL Western Blotting Substrate, Thermo Scientific, USA). Values were expressed in relation to β-actin or GAPDH (for cortex, VMH and LHA) and α-tubulin (for muscle and BAT) protein levels. For details related to antibodies and dilutions please see Reporting Summary. Uncropped images of all immunoblots are provided in Supplementary fig. 11.

Blood determinations

The quantitative determination of mouse/rat prolactin concentrations in plasma were determined by ELISA using reagents kits and methods provided by Mybiosurce (Catalog Number MBS 580033; P.R., China).

Histomorphology

BAT samples were fixed 24 hour in 10% formalin buffer and then were dehydrated and embedded in paraffin by a standard procedure. Sections of 3 μm were made in a microtome and staining in a standard Hematoxilin/Eosin Alcoholic (BioOptica) procedure following manufacturer instructions [24]. Sections were observed and photographed using a Provis AX70 microscope (Olympus, Corp, Tokyo, Japan). BAT quantification was analyzed using Image-J software (National Institutes of Health, USA).

Immunohistochemistry and immunofluorescence

Detection of UCP1 in BAT was performed using anti-UCP1 (1:500; Abcam, Cambridge, UK) and the detection was done with an anti-rabbit antibody conjugated with Alexa 488 (1:200; Molecular Probes; Grand Island, NY, USA) [24]. Images were observed and photographed using a Provis AX70 microscope (Olympus, Corp, Tokyo, Japan) and were quantified with Frida software (Framework for Image Dataset Analysis).

Animal brains were fixed by perfusion followed by inmersion-fixed in formol-calcium for 24 hours. After that were dehydrated and embedded in paraffin and using a thick section of 3 μm were cut and mounted (Vibratome Series 1000, The Vibratome Company, St Louis, MO, USA) [82]. Sections were incubated overnight at 4ºC with anti-phospho-S6 ribosomal (Cell Signaling, USA) diluted 1:200 in EnVision Flex Antibody diluent (DAKO). After washes, sections were incubated with LSAB-DAKO secondary for 30 min. Also brains were processed and immunohistochemistry assays were performed to visualize protein levels of c-FOS (Santa Cruz, CA, USA) at a dilution of 1:500 [72]. Images were observed and photographed using a Provis AX70 microscope (Olympus, Corp, Tokyo, Japan). Cellular counting was performed in the brain using Image-J software (National Institutes of Health, USA).

To test specific nuclei injection, we used immunofluorescence. To visualize green positive signals sections were incubated with rabbit antibody against green fluorescent protein (GFP) (1:200; Abcam, Cambridge, UK) and we used a goat anti-rabbit Alexa 488 (1:200; Molecular Probes; Grand Island, NY, USA).

Detection of mCherry was performed with an immunofluorescence procedure, using a rabbit anti-cherry (1:200; *Abcam*; Cambridge, UK). Detection was done with an anti-rabbit antibody conjugated with *Alexa 488* (1:200; *Molecular Probes;* Grand Island, NY, USA).

Tissue preparation, immunofluorescence and quantification were performed as described [26]. The following primary antibodies were used : mouse anti-HA (1:1000, Covance, #MMS-101R), chicken anti-GFP (1:500, Life technologies (#A10262), rabbit anti-VGlut2 (1:500, Synaptic Systems, #135402), anti-VGat (1:1000, Synaptic Systems, #131013), anti-orexin-A (1:500, Millipore, Darmstadt, Germany #AB3098) and anti-MCH (1:500, Sigma, #M8440). LHA and ZI sections were identified using a mouse

802 brain atlas and sections comprised between -1.34 to -1.70 mm from bregma were
803 analyzed.

804

805 *In situ hybridation*

806 Coronal hypothalamic sections (16 μm) were cut on a cryostat and immediately stored
807 at −80 C until hybridization. For MCH, and prepro-OX mRNA detection we employed
808 the specific antisense oligodeoxynucleotides (Table 1). These probes were 3′-end
809 labeled with [α-35S]deoxy-ATP using terminal deoxynucleotidyl transferase. The
810 frozen sections were fixed with 4% paraformaldehyde in 0.1 m phosphate buffer (pH
811 7.4) at room temperature for 30 min. They were then dehydrated using 70%, 80%, 90%,
812 95%, and absolute ethanol (5 min each). The hybridization was carried out overnight at
813 37 C in a moist chamber. Hybridization solution contained 5×10^5 (prepro-OX) or $1 \times$
814 10^6 cpm (MCH) per slide of the labeled probe, 4× standard saline citrate (SSC), 50%
815 deionized formamide, 1× Denhardt's solution, 10% dextran sulfate, and 10 μg/ml
816 sheared, single-stranded salmon sperm DNA. Afterward, the hybridization sections
817 were sequentially washed in 1× SSC at room temperature, four times in 1× SSC at 42 ºC
818 (30 min/wash), and once in 1× SSC at room temperature (1 h), and then rinsed in water
819 and ethanol. Finally, the sections were air-dried and exposed to Hyperfilm β-Max
820 (Amersham International, Little Chalfont, UK) at room temperature for 4–6 d [83]. Images
821 were quantified using Image-J software (National Institutes of Health, USA).

822

823 *Patient selection*

824 First, we conducted a retrospective chart review of patients affected by
825 hyperprolactinemia seen at the Endocrinology Department of the University Clinic of

826 Navarra between January 2007 and December 2013. All patients were of Caucasian
827 origin. Pregnant and lactating women were excluded. Patients with hyperprolactinemia
828 secondary to drugs (including neuroleptics, antidepressants, opiates and gastrointestinal
829 prokinetics) or mixed-secreting tumours or those already receiving dopamine agonists at
830 the first visit to our hospital as well as those not completing a 12-month follow-up
831 period were excluded from the analysis. Furthermore, patients with multiple pituitary
832 hormone deficiencies and/or the presence of other concomitant causes of overt
833 hypogonadism were excluded to avoid the potential effect of hormonal replacement
834 therapy on body weight control and metabolic changes. In this respect, patients with
835 previously known treatment with hypoglycemic agents to control glucose metabolism
836 abnormalities or anti-obesity drugs for body weight loss were also excluded. After all
837 the exclusions, 31 patients with newly diagnosed prolactinoma comprised the study
838 sample of the retrospective analysis (26 females and 5 males with an age range between
839 21-61 years). All patients underwent a detailed anamnesis, physical exploration and
840 metabolic evaluation (Reporting Summary). The diagnosis was based on signs and
841 symptoms of hyperprolactinemia, high serum prolactin concentrations and magnetic
842 resonance imaging (MRI) demonstrating a pituitary tumor[84]. After the diagnosis patients
843 received cabergoline, a potent long-acting dopamine agonist that is more effective and
844 better tolerated than bromocriptine[85]. Cabergoline was administered orally at a starting
845 dose of 0.25 mg once weekly at bedtime for the first week, twice weekly during the
846 second week and escalating until administration of 0.5 mg twice weekly at bedtime.
847 Prolactin normalization was achieved with this treatment protocol in all patients.

848

849 In order to examine in more detail, the potential impact of dopamine agonism on body
850 weight, body composition, resting energy expenditure and metabolic changes a

prospective study was carried out in patients affected by hyperprolactinemia seen at the same Endocrinology Department of the University Clinic of Navarra between January 2014 and May 2017 (Reporting Summary). The same inclusion and exclusion criteria and treatment protocol as for the retrospective study were applied. In this case, however, body composition as well as resting energy expenditure determinations were performed at baseline when the diagnosis was established as well as at the follow-up visits at 3, 6 and 12 months after treatment instauration with cabergoline. In the prospective study, 22 patients of Caucasian origin with newly diagnosed prolactinoma were enrolled (19 females and 3 males with an age range between 25-63 years). All patients were non-smokers and did not show signs of infection. Both clinical studies were approved, from an ethical and scientific standpoint, by the Hospital's Ethical Committee and were conducted in accordance with the principles of the Declaration of Helsinki with patients giving their informed consent for participation.

Anthropometry

Body weight was measured with a digital scale to the nearest 0.1 kg, while height was measured to the nearest 0.1 cm with a Holtain stadiometer (Holtain Ltd., Crymych, UK) to calculate the BMI. Waist circumference was determined at the midpoint between the iliac crest and the rib cage on the midaxillary line. Body fat was estimated by air-displacement-plethysmography (Bod-Pod®, Life Measurements, Concord, California, USA) [86].

Indirect calorimetry

In the prospective study the resting energy expenditure (REE) and respiratory quotient (RQ) were determined by indirect calorimetry after a 12-h overnight fast using an open-air-circuit ventilated canopy measurement system (Vmax29, SensorMedics Corporation, Yorba Linda, California) at baseline and at follow-up visits after treatment start adjusting also for body composition[87].

Blood determinations

Plasma samples were obtained by venipuncture after an overnight fast. Glucose was analyzed based on enzymatic spectrophotometric reactions by an automated analyzer (Hitachi Modular P800, Roche, Basel, Switzerland). Insulin was measured by means of an enzyme-amplified chemiluminescence assay (IMMULITE®, Diagnostic Products Corp., Los Angeles, CA). The intra-and interassay coefficients of variation (CV) were 4.2% and 5.7%, respectively. Insulin resistance was calculated using the homeostasis model assessment (HOMA-IR) index. Circulating prolactin concentrations were determined by a microparticle chemiluminescent assay (Prolactin II, Elecsys, Cobas E, Roche Diagnostics GmbH., Mannheim, Germany) with a normal range of 1-27 µg/L for women and of 1-20 µg/L for men together with intra- and interassay CV of 2.3 and 5.9%, respectively. Triglycerides, total cholesterol, high-density lipoprotein (HDL)-cholesterol and low-density lipoprotein (LDL)-cholesterol levels were calculated as previously described [88].

Statistics

Results are given as mean ± standard deviation (SD). Samples or animals were excluded whether their values were outside the ± 2-fold standard deviation [89], or whether an objective experimental failure was observed; studies were not blinded to investigators or formally randomized. The number of animals used in each study is listed in the figure legends. To test if the populations follows a Gaussian distribution, a normality test was performed (Kolgomorov-Smirnov test for n between 5-7; Shapiro-Wilk test for $n \geq 7$) [90]. For normal distributions, parametric test was used; for two population comparisons, an unpaired t tests (two-tailed for treatment and phenotyping experiment, one-tailed otherwise) were used as indicated in figure legends [91-93]; for multiple comparison test, a one-way ANOVA followed by Bonferroni *post hoc* multiple comparison test, was performed [94]. For non-Gaussian distributions was used; Man-Whitney test were used for two comparison test [95], and Kruskal-Wallis followed by Dunn *post hoc* test for multiple comparison [96,97]. Data analysis was performed using GraphPad Prism Software Version 5.0 (GraphPad, San Diego, CA). The correlation between locomotor activity and energy expenditure was analyzed by Pearson's correlation (normally distributed data) or Spearman's rank correlation (non-normally distributed data) coefficients (r). Data analysis was performed using the SPSS version 20.0 sofware statistical package (SPSS, Chicago, IL) (Reporting Summary).

In patients, comparison of changes at baseline and after treatment administration at different time points was carried out by two-tailed paired Student's *t*-tests between pre- and post-treatment values and Wilcoxon signed rank test as appropriate. The calculations were performed using the SPSS/Windows version 15.0 statistical package (SPSS, Chicago, IL) (Reporting Summary). A p value < 0.05 was considered statistically significant.

Data availability

The data that support the findings of this study are available from the corresponding author upon request. Correspondence and requests for materials should be addressed to Ruben Nogueiras.

Acknowledgments

We would like to thank Luz Casas for her excellent technical assistance. This work has been supported by grants from FEDER/Ministerio de Ciencia, Innovación y Universidades-Agencia Estatal de Investigación (CD: BFU2017-87721; ML: SAF2015-71026-R and BFU2015-70454-REDT/*Adipoplast*; RN: BFU2015-70664R), Xunta de Galicia (ML: 2015-CP079 and 2016-PG068; RN: 2015-CP080 and 2016-PG057), Fundación BBVA (RN), Fundación Atresmedia (ML and RN), Instituto de Salud Carlos III and cofounded by FEDER (LMS:PI15/01272 and PI18/01890). The research leading to these results has also received funding from the European Community's H2020 Framework Programme under the following grant: ERC Synergy Grant-2019-WATCH-810331 to VP and RN. Centro de Investigación Biomédica en Red (CIBER) de Fisiopatología de la Obesidad y Nutrición (CIBERobn). CIBERobn is an initiative of the Instituto de Salud Carlos III (ISCIII) of Spain which is supported by FEDER funds. This work was supported by Inserm, Fondation pour la Recherche Médicale, ANR-EPITRACES (EV).

Author contributions

C.F., D.B., B.P., M.D., E.P., M.F-F., S.B-F., R.G., R.H-B., C.C., A.S., P.S-C., N.G., P.A., D.G., M.F., A.R-R., I.K., and Z.L. carried out the experiments. R.A., C.B., J.L.L-B., F.J. generated viral vectors and animal models. J.S. and G.F. performed the assays in patients. C.F., V.P., C.D., M.L., E.V., L.M.S., and R.N. designed and planned the study. All authors contributed to the preparation of the manuscript.

Figure legends

Figure 1. Chronic central infusion of bromocriptine reduces diet-induced obesity. (a-d) Effect of a 14-day intracerebroventricular infusion of bromocriptine (BC) (40 µg/rat/day) and subcutaneous injection of SR59230A hydrochloride (3 mg/kg) on body weight (a), cumulative food intake (b) (n=8); representative histology of BAT lipid content and quantification of lipid droplet average area (c) (n=7), scale bars, 200 µm; protein levels of BAT UCP1, FGF21, PRDM16 and PGC1α in rats fed a chow diet (d) (n=7). (e-l) Effect of a 10-day intracerebroventricular infusion of bromocriptine (40 µg/rat/day) and subcutaneous injection of SR59230A hydrochloride (3 mg/kg) on cumulative food intake (e); body weight change (f); white mass gain (g); energy expenditure (EE) (h); respiratory quotient (RQ) (i), locomotor activity (j) (n=7 Veh, n=8 BC and n=7 BC+ SR59230A hydrochloride treatment); representative histology of BAT lipid content and quantification of lipid droplet average area (k) (n=7 each treatment), scale bars, 200 µm; protein levels of BAT UCP1, FGF21, PRDM16 and PGC1α (l) (n=7 Veh, n=8 BC and n=7 BC+ SR59230A hydrochloride treatment) in rats fed a high fat diet (HFD). (m-q) Effect of a 7-day intracerebroventricular infusion of bromocriptine (40 µg/mouse/day) on body weight change (m); cumulative food intake (n); white mass change (o); representative histology of BAT lipid content and quantification of lipid droplet average area (p) scale bars, 200 µm, and protein levels of BAT UCP1 (q) (n= 5 WT Veh and WT BC mice, n= 4 TKO Veh and n=6 TKO BC mice). Protein data were expressed in relation (%) to control (vehicle-treated) animals. α-tubulin was used to normalize protein levels. Dividing lines indicate splicings within the same gel. Values are represented as the mean ± SD. Statistical differences according to a one-way ANOVA followed by Bonferroni *post hoc* multiple comparison test (a,b,c,e,f,g,h,i,k,j), analysis of covariance (ANCOVA) with non-fat mass as covariate (h), or a Kruskal-

Wallis followed by Dunn *post hoc* test for multiple comparison (d,e,l,m,n,o,p,q). Values are represented as the mean ± SEM. *P < 0.05, **P < 0.01, ***P < 0.001 (a,f).

Figure 2. Stimulation of D2R in the LHA/ZI stimulates BAT activity. (a-e) Effect of the specific injection of bromocriptine (BC) (40 μg/rat) in the LHA/ZI on body weight change (a) and food intake (b) (n=9 each treatment); infrared thermal images and quantification of BAT interscapular temperature (c) (n=5); representative histology of BAT lipid content and quantification of lipid droplet average area (d) (n=5), scale bars, 200 μm; protein levels of BAT UCP1 (e) (n=7) after 24 hours. (f-h) Effect of the specific injection of bromocriptine (40 μg/rat) in the VMH on body weight change (f), food intake (g), and infrared thermal images and quantification of BAT interscapular temperature after 24 hours (h) (n=9 each treatment). (i-t) Representative mCherry expression in the hypothalamic LHA/ZI after stereotaxic injection of hSYN-DIO-hM3D(Gq)-mCherry AVV, scale bar 0.2 mm (i). Effect of the stereotaxical injection of hSYN-DIO-Hm3D(Gq)-mCherry AVV in the LHA/ZI of D2R-CRE mice on body weight change (j), food intake and water intake (k), infrared thermal images and quantification of BAT interscapular temperature (l), body temperature (m) (n=7 per group); respiratory quotient (n), locomotor activity (o) and energy expenditure (p) (n=5) and correlation between energy expenditure and locomotor activity in the dark phase, in the light phase and energy expenditure during 2 hours of light phase (Pearson correlation test) (q); representative histology of BAT lipid content (r) (n=6) scale bars, 200 μm; protein levels of BAT UCP1 (s), plasma prolactin levels (t) (n= 7 Veh and n=6 CNO) after 24 hours and body temperature and BAT interscapular temperature in cold exposure (4ºC) (n=9) (u). Protein data were expressed in relation (%) to control (vehicle-treated) animals. α- tubulin was used to normalize protein levels. Dividing lines

indicate splicings within the same gel. The experiments were repeated five times (i). Data are mean ± SD. Statistical differences according to a two-sided Student´s t-test (e,f,g,h,j,l,m,u) or two-sided Mann-Whitney U test (a,b,c,d,k,n,o,p,q,r,s).

Figure 3. Knock down of D2R in the LHA/ZI blunts bromocriptine-induced weight loss. (a) Representative photomicrograph of brain section showing the injection of the viral vectors that encodes GFP expression precisely placed in the LHA/ZI, scale bar, 0.1 mm and (b) D2R protein levels in the LHA/ZI 3 weeks after the viral infection (n=7 per group). (c-i) Effect of the injection of adenoviral particles encoding for GFP- or D2R-KD in the LHA/ZI of rats treated with ICV bromocriptine (BC) (40 µg/rat) on body weight change (c), food intake (d), WAT weight (e) and infrared thermal images and quantification of BAT interscapular temperature (f) (n= 6 GFP Veh, n=8 GFP BC, n=9 D2R-KD Veh and n=9 D2R-KD BC); representative histology of BAT lipid content and quantification of lipid droplet average area (g) (n=5) scale bars, 200 µm; BAT UCP1 protein levels (h) (n= 6 in each treatment) and c-FOS immunoreactive cells (IR) in the raphe pallidus (RPa) and inferior olive (IO) with representative sections (i) (Gi, gigantocellular reticular nucleus; IO, inferior olive; py, pyramidal tract; RPa, raphe pallidus; scale bar, 100 µm (n=5). (j) Double immunostaining of HA and orexin, MCH, Vgat and Vglut2 in D2R-Cre: Ribotag mice, scale bars: 100 µm, insets, 40 µm, high magnification, 8 µm). α-tubulin and β-actin were used to normalize protein levels. Protein data were expressed in relation (%) to control (vehicle-treated) animals. Dividing lines indicate splicings within the same gel. The experiments were repeated six times (a,j). Data are mean ± SD. Statistical differences on the basis of a one-way ANOVA followed by Bonferroni *post hoc* multiple comparison test (c,d,f,g) or two-tailed Student´s t-test (b,e,h,i).

Figure 4. D2R action in GABAergic neurons requires orexin to modulate BAT. (a) Photomicrograph showing the colocalization of GFP and Vglut2 in the LHA/ZI. (b-e) Effect of the injection of Ad-hSyn-DIO-EGFP or Ad-hSyn-DIO-D2R-EGFP in the LHA/ZI of vglut2-ires-cre mice on body weight change (b), food intake (c), BAT temperature (d) (n=10) and BAT UCP1 protein levels (e) (n=4). (f) Photomicrograph showing the colocalization of GFP and Vgat in the LHA/ZI. (g) Profiles from sorted non-infected/EGFP (cortex) and infected/EGFP sites (hypothalamus) and mRNA expression of Vgat, Vglut2 and Drd2 in Vgat-ires and Vglut2-ires cre mice injected with Ad-hSyn-DIO-EGFP in the LHA/ZI (n=4). (h-k) Effect of the injection of Ad-hSyn-DIO-EGFP or Ad-hSyn-DIO-D2R-EGFP in the LHA/ZI of vgat-ires-cre mice on body weight change (h), food intake (i), BAT temperature (j) (n=12) and BAT UCP1 protein levels (k) (n=4). (l-o) Effect of the injection of Ad-hSyn-DIO- EGFP or Ad-hSyn-DIO-shD2R-EGFP in the LHA/ZI of vgat-ires-cre mice on body weight change (l), food intake (m) (n=7), BAT temperature (n) and BAT UCP1 protein levels (o) (n= 6). (p-t) Effect of a 24-hour ICV injection of bromocriptine (BC) (40 μg) on body weight change (p), food intake (q), infrared thermal images and quantification of BAT temperature (r), histology of BAT lipid content and quantification of lipid droplet average area (s) (n=4); and BAT UCP1 protein levels (t) in wild type (n=4) and orexin knockout (n=6) mice. (u-x) Effect of the injection of AAV-hSYN-DIO-Hm3D(Gq)-mCherry and the ICV injection of the orexin receptor antagonist SB-334867 (4 μg) on body weight change (u) and infrared thermal images and quantification of BAT temperature (v) (n=5-6); histology of BAT lipid content and quantification of lipid droplet average area (w) and immunostaining of UCP1 and quantification in BAT (x) (n=8) after 24 hours. Dividing lines indicate splicings within the same gel. The experiments were repeated six times (a,h). Data are mean ± SD. Statistical differences

on the basis of a two-tailed Student´s t-test (b,c,d,h,i,j,k), a Kruskal-Wallis followed by Dunn *post hoc* test for multiple comparison (c,p,q), two-way ANOVA (r), two-sided Mann-Whitney U test (e,g,l,m,n,o,s,t) or a one-way ANOVA followed by Bonferroni *post hoc* multiple comparison test (u,v,w,x).

Figure 5. Protein kinase A mediates the effects of bromocriptine on BAT. (a-d) Phosphorylated levels of CREB in the LHA/ZI after: 2-hour ICV (a) and 24-hour specific injection of bromocriptine (BC) (40 µg) in the LHA/ZI (n=7) (b); injection of AAV-hSYN-DIO-hM3D (Gq)-mCherry and the ICV injection of SB-334867 (4 µg) (n=5-6) (c); ICV injection of orexin (OX) (10 µg) and SB-334867 (4 µg) after 24 hours (n=5-9) (d). (e-j) Effect of the ICV injection of BC (40 µg) and Sp-cAMPS (90 ng) on body weight change (e), food intake (f) and white mass gain (g) (n= 9); and BAT temperature (h) (n=7-8); histology of BAT lipid content and quantification of lipid droplet area (i) and immunostaining of UCP1 and quantification in BAT (j) (n=7) after 24 hours. (k-p) Effect of the LHA/ZI injection of the specific PKA inhibitor H-89 (62 ng) on body weight change (k), food intake (l), white mass gain (m), and BAT temperature (n) (n=11-12); histology of BAT lipid content and quantification of lipid droplet area (o) (n= 10), and protein levels of BAT UCP1 (p) (n=7) after 24 hours. (q) Effect of the injection of AAV-hSyn-DIO-hM3D (Gq)-mCherry in the LHA/ZI of D2R-cre mice on PDE3B levels in the LHA/ZI (n=6). (r-s) Effect of the ICV injection of Cilostamide (10 µg) on body weight (r) and food intake (s) (n=7). (t-v) Effect of the injection of AAV-hSyn-DIO-Hm3D (Gq)-mCherry in the LHA/ZI of D2R-cre mice and the ICV injection of Cilostamide (10 µg) on body weight (t), food intake (u) and BAT temperature (v) (n=6). (w-z) Effect of the injection of Ad-hSyn-DIO-EGFP or Ad-hSyn-DIO-D2R-EGFP in the LHA/ZI of Vgat-ires-cre mice and ICV Cilostamide (10

µg) on body weight (w), food intake (x), BAT temperature (y) and energy expenditure (EE) after 24hours (z) (n= 7-8). Dividing lines indicate splicings within the same gel. Data are mean ± SD. Statistical differences according to a two-tailed Student´s t-test (a,b,q,r,s), a one-way ANOVA followed by Bonferroni *post hoc* multiple comparison test (c,e,f,g,h,i,j,w,x,y), a Kruskal-Wallis followed by Dunn *post hoc* test for multiple comparison (d, t,u,v,) or two-sided Mann-Whitney U test (k,l,m,n,o,p) and analysis of covariance (ANCOVA) with body weight as covariate (z).

Figure 6. S6 mediates the effects of bromocriptine on BAT. (a-i) rpS6 phosphorylated levels in the LHA/ZI after: ICV injection of bromocriptine (BC) (40 µg) assessed by immunohistochemistry (n=7) (a) and western blot (n=4) (b); 24-hour specific injection of BC (40 µg) in the LHA/ZI (n=7) (c); injection of Ad-GFP or Ad-shD2R in the LHA/ZI of rats treated with ICV bromocriptine (40 µg) (n= 6 GFP Veh, n=7 GFP BC, n=7 D2R-KD Veh and n=7 D2R-KD BC) (d); 24-hour ICV injection of BC (40 µg) in wild type (n=4) and orexin (OX) knockout mice (n=6) (e); injection of AAV-hSYN-DIO-hM3D (Gq)-mCherry and the ICV injection of SB-334867 (4 µg) (n=4 Veh, n=4 CNO and n=5 CNO+SB-334867) (f); ICV injection of OX (10 µg) and SB-334867 (4 µg) (n=6) (g); LHA/ZI injection of the specific PKA inhibitor H-89 (62 ng) (n=7) (h); and ICV injection of BC (40 µg) and the specific PKA activator Sp-cAMPS (90 ng) after 24 hours (n=6) (i). (j) Total and rpS6 phosphorylated levels in the LHA/ZI 3 weeks after the viral infection (n=7). (k-o) Effect of the injection of adenoviral particles encoding for Null or S6K1 in the LHA/ZI of rats treated with ICV BC (40 µg) on body weight change (k), food intake (l) and infrared thermal images and quantification of BAT interscapular temperature (m) (n= 8 ad null Veh, n=9 ad null BC, n=8 ad S6K1 Veh and n=9 ad S6K1 BC), histology of BAT lipid content and

quantification of lipid droplet average area (n), and BAT UCP1 protein levels (o) (n=7). Dividing lines indicate splicings within the same gel. Data are mean ± SD. Statistical differences according to a two-tailed Student´s t-test (a,c,d), a two-sided Man-Whitney test (b,e,h,j), a Kruskal-Wallis followed by Dunn *post hoc* test for multiple comparison (f,g,i) or a one-way ANOVA followed by Bonferroni *post hoc* multiple comparison test (k,l,m,n,o).

Figure 7. Cabergoline decreases body weight and increases resting energy expenditure in patients. (a) Waterfall plot of the body weight changes experimented by each patient (1-31) of the retrospective study between baseline and following 0.5 mg twice weekly cabergoline treatment for 12 months. (b) Waterfall plot of the body weight changes experimented by each patient (1-21) of the prospective study during the first 3 months of cabergoline treatment instauration with 0.5 mg cabergoline twice weekly. (c) REE in patients before and after cabergoline treatment compared to the REE predicted from the Harris Benedict equation. (d) Correlation between REE and weight loss in patients treated with cabergoline.

Table 1. Clinical, anthropometric and metabolic characteristics of hyperprolactinemic patients before and after one year of treatment initiation with cabergoline.

Condition/Variable	Patient at diagnosis	Cabergoline treatment	Stat signif.
(n = 31)	**Baseline**	**After 12 months**	**P value**
Gender (m/f)	5/26	5/26	0.732
Age (years)	35 ± 10	36 ± 11	0.846
Body weight (kg)	67.5 ± 17.1	64.3 ± 14.2	0.045
BMI (kg/m^2)	24.9 ± 5.4	23.8 ± 4.6	0.043
Prolactin (μg/L)	99.5 ± 16.7	8.3 ± 9	<0.001
Glucose (mmol/L)	5.8 ± 1.7	4.6 ± 1.5	0.038
Insulin (pmol/L)	92 ± 48	79 ± 54	0.040
HOMA-IR	3.32 ± 2.15	2.26 ± 1.38	0.039
Triglycerides (mmol/L)	2.0 ± 0.9	1.3 ± 0.5	0.008
Total cholesterol (mmol/L)	5.0 ± 1.1	4.2 ± 0.6	0.041
LDL cholesterol (mmol/L)	3.2 ± 1.0	2.1 ± 0.7	0.033
HDL cholesterol (mmol/L)	1.1 ± 0.4	1.4 ± 0.5	0.075

Condition/Variable	Patient at	Cabergoline treatment		Stat. signif. P value	
(n = 21)	**Baseline**	**3 months**	**12 months**	**(a)**	**(b)**
Gender (m/f)	3/18	3/18	3/18	0.806	
Age (years)	40 + 12	40 + 12	41 + 11	0.799	
Body weight (kg)	70.5 ± 10.6	64.6 ± 12.3	64.1 ± 15.0	0.044	0.045
BMI (kg/m^2)	25.8 ± 5.1	24.2 ± 4.2	23.6 ± 5.3	0.042	0.043
WC (cm)	90 ± 11	84 ± 9	83 ± 10	0.047	0.046
Body fat (%)	34.7 ± 5.6	29.5 ± 4.2	28.9 ± 6.1	0.040	0.039
REE (kJ/d)	5997 ± 704	6703 ± 800	6532 ± 779	0.046	0.045
REE (kJ/kg/d)	85.1 ± 9.2	104.2 ± 9.8	102.7 ± 8.6	0.041	0.040
REE (kJ/kg FFM/d)	90.0 ± 7.7	105.4 ± 5.6	101.9 ± 6.3	0.037	0.038
RQ (vCO_2/vO_2)	0.83 ± 0.06	0.84 ± 0.05	0.83 ± 0.08	0.621	0.665
Prolactin (μg/L)	111.5 ± 12.7	9.3 ± 3.1	8.3 ± 5.0	<0.001	<0.001
Glucose (mmol/L)	5.7 ± 0.8	4.1 ± 0.3	4.5 ± 0.5	0.042	0.04
Insulin (pmol/L)	93 ± 56	71 ± 44	75 ± 52	0.037	0.036
HOMA-IR	3.53 ± 1.98	2.15 ± 1.59	2.43 ± 1.80	0.038	0.039
Triglycerides (mmol/L)	2.1 ± 1.0	1.1 ± 0.3	1.3 ± 0.4	0.022	0.026
Total cholesterol (mmol/L)	5.0 ± 0.9	4.7 ± 0.8	4.9 ± 1.0	0.278	0.301
LDL cholesterol (mmol/L)	3.0 ± 1.1	2.5 ± 0.6	2.6 ± 0.8	0.293	0.352
HDL cholesterol (mmol/L)	1.0 ± 0.6	1.2 ± 0.7	1.1 ± 0.5	0.348	0.386

BMI, body mass index; WC, waist circumference; REE, resting energy expenditure; RQ, respiratory quotient; vCO_2/vO_2, dimensionless ratio between carbon dioxide production and oxygen consumption; HOMA-IR, homeostatic model assessment. Data are mean ± SD; comparison of baseline with (a) 3 months following cabergoline treatment initiation and (b) 12 months after cabergoline treatment start; according to a two-sided Student's *t*-tests between pre- and post-treatment values and Wilcoxon signed rank test.

REFERENCES

1. Palmiter, R.D. Is dopamine a physiologically relevant mediator of feeding behavior? *Trends in neurosciences* **30**, 375-381 (2007).
2. Mirmohammadsadeghi, Z., Shareghi Brojeni, M., Haghparast, A. & Eliassi, A. Role of paraventricular hypothalamic dopaminergic D1 receptors in food intake regulation of food-deprived rats. *European journal of pharmacology* **818**, 43-49 (2018).
3. Zhu, X., Ottenheimer, D. & DiLeone, R.J. Activity of D1/2 Receptor Expressing Neurons in the Nucleus Accumbens Regulates Running, Locomotion, and Food Intake. *Frontiers in behavioral neuroscience* **10**, 66 (2016).
4. Land, B.B.*, et al.* Medial prefrontal D1 dopamine neurons control food intake. *Nature neuroscience* **17**, 248-253 (2014).
5. Fetissov, S.O., Meguid, M.M., Sato, T. & Zhang, L.H. Expression of dopaminergic receptors in the hypothalamus of lean and obese Zucker rats and food intake. *American journal of physiology. Regulatory, integrative and comparative physiology* **283**, R905-910 (2002).
6. Johnson, P.M. & Kenny, P.J. Dopamine D2 receptors in addiction-like reward dysfunction and compulsive eating in obese rats. *Nature neuroscience* **13**, 635-641 (2010).
7. Volkow, N.D., Wang, G.J. & Baler, R.D. Reward, dopamine and the control of food intake: implications for obesity. *Trends in cognitive sciences* **15**, 37-46 (2011).
8. Wang, G.J., Volkow, N.D. & Fowler, J.S. The role of dopamine in motivation for food in humans: implications for obesity. *Expert opinion on therapeutic targets* **6**, 601-609 (2002).
9. Holt, R.I., Barnett, A.H. & Bailey, C.J. Bromocriptine: old drug, new formulation and new indication. *Diabetes, obesity & metabolism* **12**, 1048-1057 (2010).
10. Cincotta, A.H. & Meier, A.H. Bromocriptine (Ergoset) reduces body weight and improves glucose tolerance in obese subjects. *Diabetes care* **19**, 667-670 (1996).
11. Pijl, H.*, et al.* Bromocriptine: a novel approach to the treatment of type 2 diabetes. *Diabetes care* **23**, 1154-1161 (2000).
12. Gaziano, J.M.*, et al.* Randomized clinical trial of quick-release bromocriptine among patients with type 2 diabetes on overall safety and cardiovascular outcomes. *Diabetes care* **33**, 1503-1508 (2010).
13. Wang, G.J.*, et al.* Brain dopamine and obesity. *Lancet* **357**, 354-357 (2001).
14. Bray, G.A., Fruhbeck, G., Ryan, D.H. & Wilding, J.P. Management of obesity. *Lancet* **387**, 1947-1956 (2016).
15. Henderson, D.C., Vincenzi, B., Andrea, N.V., Ulloa, M. & Copeland, P.M. Pathophysiological mechanisms of increased cardiometabolic risk in people with schizophrenia and other severe mental illnesses. *The lancet. Psychiatry* **2**, 452-464 (2015).
16. Noble, E.P.*, et al.* D2 dopamine receptor gene and obesity. *The International journal of eating disorders* **15**, 205-217 (1994).
17. Sun, X., Luquet, S. & Small, D.M. DRD2: Bridging the Genome and Ingestive Behavior. *Trends in cognitive sciences* **21**, 372-384 (2017).
18. Meier, A.H., Cincotta, A.H. & Lovell, W.C. Timed bromocriptine administration reduces body fat stores in obese subjects and hyperglycemia in type II diabetics. *Experientia* **48**, 248-253 (1992).
19. Gibson, C.D., Karmally, W., McMahon, D.J., Wardlaw, S.L. & Korner, J. Randomized pilot study of cabergoline, a dopamine receptor agonist: effects on body weight and glucose tolerance in obese adults. *Diabetes, obesity & metabolism* **14**, 335-340 (2012).

20. Liu, X*., et al.* The Mechanism and Pathways of Dopamine and Dopamine Agonists in Prolactinomas. *Frontiers in endocrinology* **9**, 768 (2018).
21. Al-Massadi, O*., et al.* Pharmacological and Genetic Manipulation of p53 in Brown Fat at Adult But Not Embryonic Stages Regulates Thermogenesis and Body Weight in Male Mice. *Endocrinology* **157**, 2735-2749 (2016).
22. Fruhbeck, G., Mendez-Gimenez, L., Fernandez-Formoso, J.A., Fernandez, S. & Rodriguez, A. Regulation of adipocyte lipolysis. *Nutrition research reviews* **27**, 63-93 (2014).
23. Hankir, M.K., Cowley, M.A. & Fenske, W.K. A BAT-Centric Approach to the Treatment of Diabetes: Turn on the Brain. *Cell metabolism* **24**, 31-40 (2016).
24. Folgueira, C*., et al.* Uroguanylin Action in the Brain Reduces Weight Gain in Obese Mice via Different Efferent Autonomic Pathways. *Diabetes* **65**, 421-432 (2016).
25. Martinez-Sanchez, N*., et al.* Hypothalamic AMPK-ER Stress-JNK1 Axis Mediates the Central Actions of Thyroid Hormones on Energy Balance. *Cell metabolism* **26**, 212-229 e212 (2017).
26. Weiner, D.M*., et al.* D1 and D2 dopamine receptor mRNA in rat brain. *Proceedings of the National Academy of Sciences of the United States of America* **88**, 1859-1863 (1991).
27. Gomez, J.L*., et al.* Chemogenetics revealed: DREADD occupancy and activation via converted clozapine. *Science* **357**, 503-507 (2017).
28. Stagkourakis, S., Kim, H., Lyons, D.J. & Broberger, C. Dopamine Autoreceptor Regulation of a Hypothalamic Dopaminergic Network. *Cell reports* **15**, 735-747 (2016).
29. Puighermanal, E*., et al.* drd2-cre:ribotag mouse line unravels the possible diversity of dopamine d2 receptor-expressing cells of the dorsal mouse hippocampus. *Hippocampus* **25**, 858-875 (2015).
30. Segal-Lieberman, G*., et al.* Melanin-concentrating hormone is a critical mediator of the leptin-deficient phenotype. *Proceedings of the National Academy of Sciences of the United States of America* **100**, 10085-10090 (2003).
31. Tupone, D., Madden, C.J., Cano, G. & Morrison, S.F. An orexinergic projection from perifornical hypothalamus to raphe pallidus increases rat brown adipose tissue thermogenesis. *The Journal of neuroscience : the official journal of the Society for Neuroscience* **31**, 15944-15955 (2011).
32. Martins, L*., et al.* A Functional Link between AMPK and Orexin Mediates the Effect of BMP8B on Energy Balance. *Cell reports* **16**, 2231-2242 (2016).
33. Yamaguchi, T*., et al.* Role of PKA signaling in D2 receptor-expressing neurons in the core of the nucleus accumbens in aversive learning. *Proceedings of the National Academy of Sciences of the United States of America* **112**, 11383-11388 (2015).
34. Bonito-Oliva, A*., et al.* Haloperidol promotes mTORC1-dependent phosphorylation of ribosomal protein S6 via dopamine- and cAMP-regulated phosphoprotein of 32 kDa and inhibition of protein phosphatase-1. *Neuropharmacology* **72**, 197-203 (2013).
35. Mighiu, P.I*., et al.* Hypothalamic glucagon signaling inhibits hepatic glucose production. *Nature medicine* **19**, 766-772 (2013).
36. Quinones, M*., et al.* Hypothalamic CaMKKbeta mediates glucagon anorectic effect and its diet-induced resistance. *Molecular metabolism* **4**, 961-970 (2015).
37. Meacci, E*., et al.* Molecular cloning and expression of human myocardial cGMP-inhibited cAMP phosphodiesterase. *Proceedings of the National Academy of Sciences of the United States of America* **89**, 3721-3725 (1992).
38. Zhao, A.Z., Huan, J.N., Gupta, S., Pal, R. & Sahu, A. A phosphatidylinositol 3-kinase phosphodiesterase 3B-cyclic AMP pathway in hypothalamic action of leptin on feeding. *Nature neuroscience* **5**, 727-728 (2002).

39. Sahu, M., Anamthathmakula, P. & Sahu, A. Hypothalamic Phosphodiesterase 3B Pathway Mediates Anorectic and Body Weight-Reducing Effects of Insulin in Male Mice. *Neuroendocrinology* **104**, 145-156 (2017).
40. Sahu, M., Anamthathmakula, P. & Sahu, A. Phosphodiesterase-3B-cAMP pathway of leptin signalling in the hypothalamus is impaired during the development of diet-induced obesity in FVB/N mice. *Journal of neuroendocrinology* **27**, 293-302 (2015).
41. Moore, C.E., Xie, J., Gomez, E. & Herbert, T.P. Identification of cAMP-dependent kinase as a third in vivo ribosomal protein S6 kinase in pancreatic beta-cells. *Journal of molecular biology* **389**, 480-494 (2009).
42. Valjent, E*., et al.* Haloperidol regulates the state of phosphorylation of ribosomal protein S6 via activation of PKA and phosphorylation of DARPP-32. *Neuropsychopharmacology : official publication of the American College of Neuropsychopharmacology* **36**, 2561-2570 (2011).
43. Blouet, C., Ono, H. & Schwartz, G.J. Mediobasal hypothalamic p70 S6 kinase 1 modulates the control of energy homeostasis. *Cell metabolism* **8**, 459-467 (2008).
44. Richard, D. Cognitive and autonomic determinants of energy homeostasis in obesity. *Nature reviews. Endocrinology* **11**, 489-501 (2015).
45. Meguid, M.M., Yang, Z.J. & Montante, A. Lateral hypothalamic dopaminergic neural activity in response to total parenteral nutrition. *Surgery* **114**, 400-405; discussion 405-406 (1993).
46. Meguid, M.M., Yang, Z.J. & Koseki, M. Eating induced rise in LHA-dopamine correlates with meal size in normal and bulbectomized rats. *Brain research bulletin* **36**, 487-490 (1995).
47. Yang, Z.J., Koseki, M., Meguid, M.M. & Laviano, A. Eating-related increase of dopamine concentration in the LHA with oronasal stimulation. *The American journal of physiology* **270**, R315-318 (1996).
48. Najam, N. Involvement of dopaminergic systems in the ventromedial hypothalamic hyperphagia. *Brain research bulletin* **21**, 571-574 (1988).
49. Baptista, T., Parada, M. & Hernandez, L. Long term administration of some antipsychotic drugs increases body weight and feeding in rats. Are D2 dopamine receptors involved? *Pharmacology, biochemistry, and behavior* **27**, 399-405 (1987).
50. Meguid, M.M., Yang, Z.J. & Laviano, A. Meal size and number: relationship to dopamine levels in the ventromedial hypothalamic nucleus. *The American journal of physiology* **272**, R1925-1930 (1997).
51. Meguid, M.M*., et al.* Hypothalamic dopamine and serotonin in the regulation of food intake. *Nutrition* **16**, 843-857 (2000).
52. Zhang, X. & van den Pol, A.N. Hypothalamic arcuate nucleus tyrosine hydroxylase neurons play orexigenic role in energy homeostasis. *Nature neuroscience* **19**, 1341-1347 (2016).
53. Labouesse, M.A*., et al.* Striatal dopamine 2 receptor upregulation during development predisposes to diet-induced obesity by reducing energy output in mice. *Proceedings of the National Academy of Sciences of the United States of America* **115**, 10493-10498 (2018).
54. Carlin, J., Hill-Smith, T.E., Lucki, I. & Reyes, T.M. Reversal of dopamine system dysfunction in response to high-fat diet. *Obesity* **21**, 2513-2521 (2013).
55. Friend, D.M*., et al.* Basal Ganglia Dysfunction Contributes to Physical Inactivity in Obesity. *Cell metabolism* **25**, 312-321 (2017).
56. Lopez, M., Nogueiras, R., Tena-Sempere, M. & Dieguez, C. Hypothalamic AMPK: a canonical regulator of whole-body energy balance. *Nature reviews. Endocrinology* **12**, 421-432 (2016).
57. Kohlie, R*., et al.* Dopamine directly increases mitochondrial mass and thermogenesis in brown adipocytes. *Journal of molecular endocrinology* **58**, 57-66 (2017).

58. Burt, J., Alberto, C.O., Parsons, M.P. & Hirasawa, M. Local network regulation of orexin neurons in the lateral hypothalamus. *American journal of physiology. Regulatory, integrative and comparative physiology* **301**, R572-580 (2011).
59. Bubser, M.*, et al.* Dopaminergic regulation of orexin neurons. *The European journal of neuroscience* **21**, 2993-3001 (2005).
60. Yasuda, T.*, et al.* Dual regulatory effects of orexins on sympathetic nerve activity innervating brown adipose tissue in rats. *Endocrinology* **146**, 2744-2748 (2005).
61. Sellayah, D., Bharaj, P. & Sikder, D. Orexin is required for brown adipose tissue development, differentiation, and function. *Cell metabolism* **14**, 478-490 (2011).
62. Stoof, J.C. & Kebabian, J.W. Opposing roles for D-1 and D-2 dopamine receptors in efflux of cyclic AMP from rat neostriatum. *Nature* **294**, 366-368 (1981).
63. Yang, L. & McKnight, G.S. Hypothalamic PKA regulates leptin sensitivity and adiposity. *Nature communications* **6**, 8237 (2015).
64. Cummings, D.E.*, et al.* Genetically lean mice result from targeted disruption of the RII beta subunit of protein kinase A. *Nature* **382**, 622-626 (1996).
65. Zheng, R.*, et al.* Deficiency of the RIIbeta subunit of PKA affects locomotor activity and energy homeostasis in distinct neuronal populations. *Proceedings of the National Academy of Sciences of the United States of America* **110**, E1631-1640 (2013).
66. Inancli, S.S.*, et al.* Effect of cabergoline on insulin sensitivity, inflammation, and carotid intima media thickness in patients with prolactinoma. *Endocrine* **44**, 193-199 (2013).
67. Pala, N.A., Laway, B.A., Misgar, R.A. & Dar, R.A. Metabolic abnormalities in patients with prolactinoma: response to treatment with cabergoline. *Diabetology & metabolic syndrome* **7**, 99 (2015).
68. Lamos, E.M., Levitt, D.L. & Munir, K.M. A review of dopamine agonist therapy in type 2 diabetes and effects on cardio-metabolic parameters. *Prim Care Diabetes* **10**, 60-65 (2016).
69. Nogueiras, R.*, et al.* Direct control of peripheral lipid deposition by CNS GLP-1 receptor signaling is mediated by the sympathetic nervous system and blunted in diet-induced obesity. *The Journal of neuroscience : the official journal of the Society for Neuroscience* **29**, 5916-5925 (2009).
70. Nogueiras, R.*, et al.* The central melanocortin system directly controls peripheral lipid metabolism. *The Journal of clinical investigation* **117**, 3475-3488 (2007).
71. Gangarossa, G.*, et al.* Characterization of dopamine D1 and D2 receptor-expressing neurons in the mouse hippocampus. *Hippocampus* **22**, 2199-2207 (2012).
72. Beiroa, D.*, et al.* GLP-1 agonism stimulates brown adipose tissue thermogenesis and browning through hypothalamic AMPK. *Diabetes* **63**, 3346-3358 (2014).
73. Contreras, C.*, et al.* Central ceramide-induced hypothalamic lipotoxicity and ER stress regulate energy balance. *Cell reports* **9**, 366-377 (2014).
74. Czyzyk, T.A.*, et al.* Mice lacking delta-opioid receptors resist the development of diet-induced obesity. *FASEB journal : official publication of the Federation of American Societies for Experimental Biology* **26**, 3483-3492 (2012).
75. Alvarez-Crespo, M.*, et al.* Essential role of UCP1 modulating the central effects of thyroid hormones on energy balance. *Molecular metabolism* **5**, 271-282 (2016).
76. Imbernon, M.*, et al.* Hypothalamic kappa opioid receptor mediates both diet-induced and melanin concentrating hormone-induced liver damage through inflammation and endoplasmic reticulum stress. *Hepatology* **64**, 1086-1104 (2016).
77. Alvarez-Crespo, M.*, et al.* The orexigenic effect of orexin-A revisited: dependence of an intact growth hormone axis. *Endocrinology* **154**, 3589-3598 (2013).
78. de Jong, J.W.*, et al.* Reducing Ventral Tegmental Dopamine D2 Receptor Expression Selectively Boosts Incentive Motivation. *Neuropsychopharmacology : official publication of the American College of Neuropsychopharmacology* **40**, 2085-2095 (2015).

79. Messina, A.*, et al.* A microRNA switch regulates the rise in hypothalamic GnRH production before puberty. *Nature neuroscience* **19**, 835-844 (2016).
80. Konner, A.C.*, et al.* Insulin action in AgRP-expressing neurons is required for suppression of hepatic glucose production. *Cell metabolism* **5**, 438-449 (2007).
81. Lopez, M.*, et al.* Hypothalamic AMPK and fatty acid metabolism mediate thyroid regulation of energy balance. *Nature medicine* **16**, 1001-1008 (2010).
82. Imbernon, M.*, et al.* Central melanin-concentrating hormone influences liver and adipose metabolism via specific hypothalamic nuclei and efferent autonomic/JNK1 pathways. *Gastroenterology* **144**, 636-649 e636 (2013).
83. Seoane, L.M.*, et al.* Agouti-related peptide, neuropeptide Y, and somatostatin-producing neurons are targets for ghrelin actions in the rat hypothalamus. *Endocrinology* **144**, 544-551 (2003).
84. Melmed, S.*, et al.* Diagnosis and treatment of hyperprolactinemia: an Endocrine Society clinical practice guideline. *J. Clin. Endocrinol. Metab.* **96**, 273-288 (2011).
85. Webster, J.*, et al.* A comparison of cabergoline and bromocriptine in the treatment of hyperprolactinemic amenorrhea. Cabergoline Comparative Study Group. *N. Engl. J. Med.* **331**, 904-909 (1994).
86. Gómez-Ambrosi, J.*, et al.* Body adiposity and type 2 diabetes: increased risk with a high body fat percentage even having a normal BMI. *Obesity* **19**, 1439-1444 (2011).
87. Sabater, M.*, et al.* Circulating pigment epithelium-derived factor levels are associated with insulin resistance and decrease after weight loss. *J. Clin. Endocrinol. Metab.* **95**, 4720-4728 (2010).
88. Gómez-Ambrosi, J.*, et al.* Involvement of leptin in the association between percentage of body fat and cardiovascular risk factors. *Clin. Biochem.* **35**, 315-320 (2002).
89. Miller, J. Reaction time analysis with outlier exclusion: bias varies with sample size. *The Quarterly journal of experimental psychology. A, Human experimental psychology* **43**, 907-912 (1991).
90. Razali, N.M. & Wah, Y.B. Power comparisons of shapiro-wilk, kolmogorov-smirnov, lilliefors and anderson-darling tests. *Journal of Statistical Modeling and Analytics* **2**, 21-33 (2011).
91. Student. The probable error of a mean. *Biometrika* **6**, 1-25 (1908).
92. Fay, D.S. & Gerow, K. A biologist's guide to statistical thinking and analysis (). *WormBook : the online review of C. elegans biology*, 10.1895/wormbook.1891.1159.1891 (2013).
93. Charan, J. & Biswas, T. How to Calculate Sample Size for Different Study Designs in Medical Research? *Indian Journal of Psychological Medicine* **35**, 121-126 (2013).
94. Kao, L.S. & Green, C.E. Analysis of Variance: Is There a Difference in Means and What Does It Mean? *The Journal of surgical research* **144**, 158-170 (2008).
95. Bridge, P.D. & Sawilowsky, S.S. Increasing Physicians' Awareness of the Impact of Statistics on Research Outcomes. *Journal of Clinical Epidemiology* **52**, 229-235 (1999).
96. Dunn, O.J. Multiple Comparisons Using Rank Sums. *Technometrics* **6**, 241-252 (1964).
97. Campbell, G. & Skillings, J.H. Nonparametric Stepwise Multiple Comparison Procedures. *Journal of the American Statistical Association* **80**, 998-1003 (1985).

Figure 1

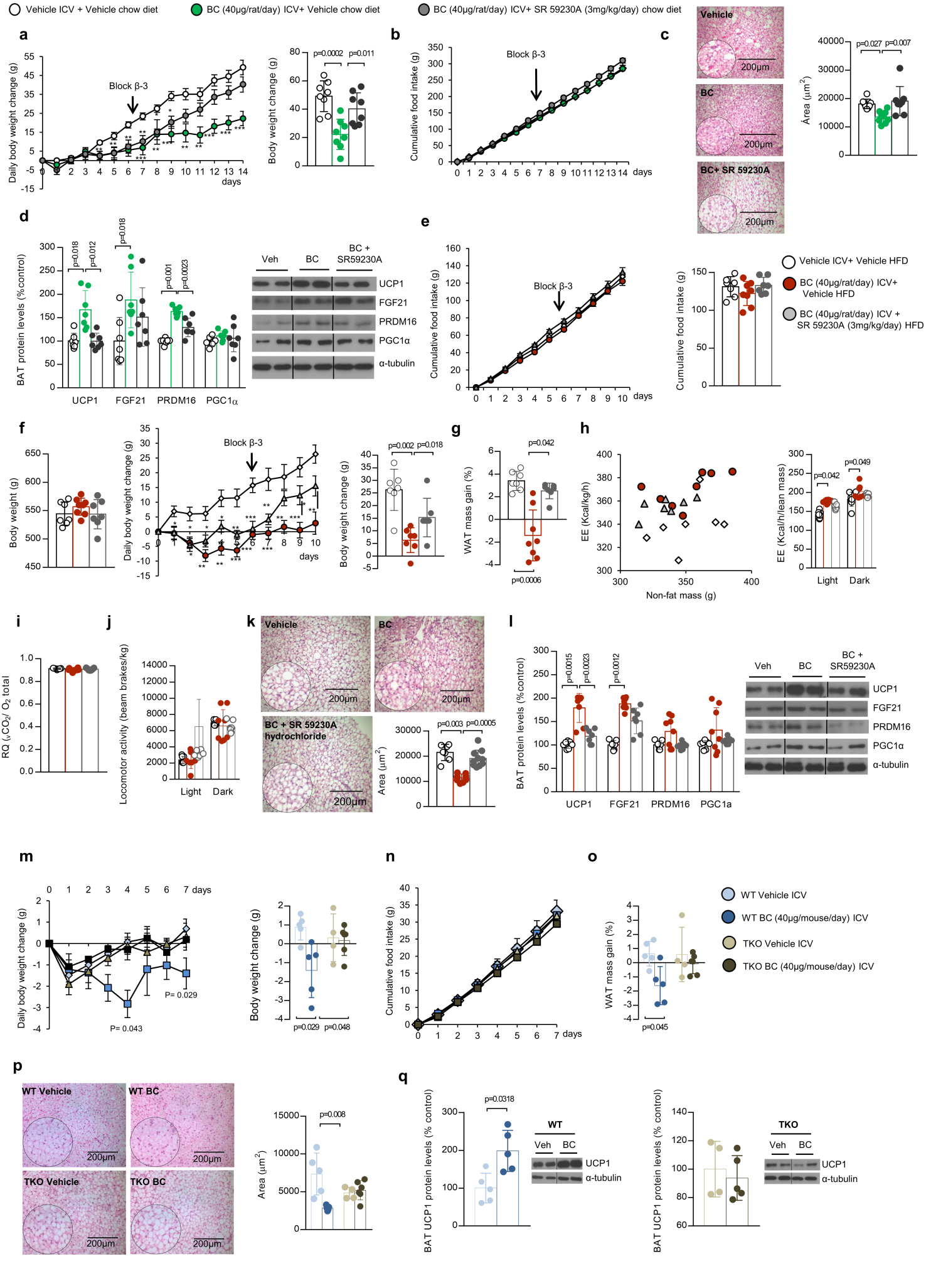
Vehicle ICV + Vehicle chow diet
BC (40µg/rat/day) ICV+ Vehicle chow diet
BC (40µg/rat/day) ICV+ SR 59230A (3mg/kg/day) chow diet
a
Daily body weight change (g)
Block β-3
days
Body weight change (g)
p=0.0002
p=0.011
b
Cumulative food intake (g)
Block β-3
days
c
Vehicle
BC
BC+ SR 59230A
200µm
Area (µm²)
p=0.027
p=0.007
d
BAT protein levels (%control)
p=0.018
p=0.012
p=0.018
p=0.001
p=0.0023
UCP1
FGF21
PRDM16
PGC1α
Veh
BC
BC + SR59230A
α-tubulin
e
Cumulative food intake (g)
Block β-3
days
Vehicle ICV+ Vehicle HFD
BC (40µg/rat/day) ICV+ Vehicle HFD
BC (40µg/rat/day) ICV + SR 59230A (3mg/kg/day) HFD
f
Body weight (g)
Daily body weight change (g)
Block β-3
days
Body weight change (g)
p=0.002
p=0.018
g
WAT mass gain (%)
p=0.042
p=0.0006
h
EE (Kcal/kg/h)
Non-fat mass (g)
EE (Kcal/h/lean mass)
p=0.042
p=0.049
Light
Dark
i
RQ (vCO2/ O2 total
j
Locomotor activity (beam brakes/kg)
Light
Dark
k
Vehicle
BC
BC + SR 59230A hydrochloride
200µm
Area (µm²)
p=0.003
p=0.0005
l
BAT protein levels (%control)
p=0.0015
p=0.0023
p=0.0012
UCP1
FGF21
PRDM16
PGC1a
Veh
BC
BC + SR59230A
α-tubulin
m
Daily body weight change (g)
0 1 2 3 4 5 6 7 days
P= 0.029
P= 0.043
Body weight change (g)
p=0.029
p=0.048
n
Cumulative food intake (g)
days
o
WAT mass gain (%)
p=0.045
WT Vehicle ICV
WT BC (40µg/mouse/day) ICV
TKO Vehicle ICV
TKO BC (40µg/mouse/day) ICV
p
WT Vehicle
WT BC
TKO Vehicle
TKO BC
200µm
Area (µm²)
p=0.008
q
BAT UCP1 protein levels (% control)
p=0.0318
WT
Veh
BC
UCP1
α-tubulin
TKO
Veh
BC
UCP1
α-tubulin

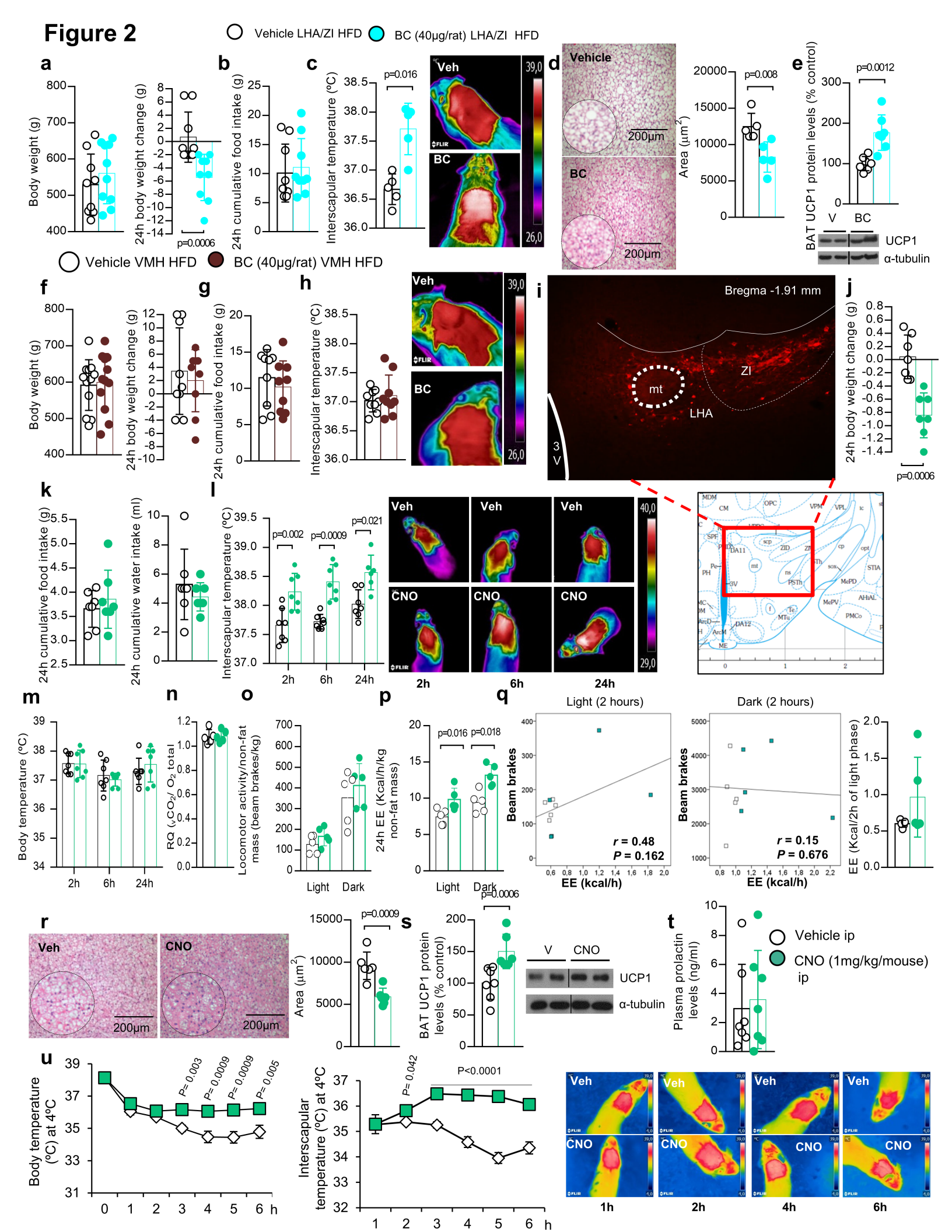
Figure 2
Vehicle LHA/ZI HFD
BC (40µg/rat) LHA/ZI HFD
Vehicle VMH HFD
BC (40µg/rat) VMH HFD
a
b
c
d
e
f
g
h
i
j
k
l
m
n
o
p
q
r
s
t
u
Body weight (g)
24h body weight change (g)
24h cumulative food intake (g)
Interscapular temperature (ºC)
Area (µm²)
BAT UCP1 protein levels (% control)
24h cumulative water intake (ml)
Body temperature (ºC)
RQ (vCO2/ VO2 total
Locomotor activity/non-fat mass (beam brakes/kg)
24h EE (Kcal/h/kg non-fat mass)
Beam brakes
EE (kcal/h)
EE (Kcal/2h of light phase)
Plasma prolactin levels (ng/ml)
Body temperature (ºC) at 4ºC
Interscapular temperature (ºC) at 4ºC
Veh
CNO
BC
Vehicle
UCP1
α-tubulin
Bregma -1.91 mm
mt
ZI
LHA
Light (2 hours)
Dark (2 hours)
r = 0.48
P = 0.162
r = 0.15
P = 0.676
Vehicle ip
CNO (1mg/kg/mouse) ip
200µm
p=0.016
p=0.0006
p=0.008
p=0.0012
p=0.002
p=0.0009
p=0.021
p=0.018
P= 0.003
P= 0.0009
P= 0.0009
P= 0.005
P= 0.042
P<0.0001
2h
6h
24h
1h
4h
Light
Dark

Figure 3

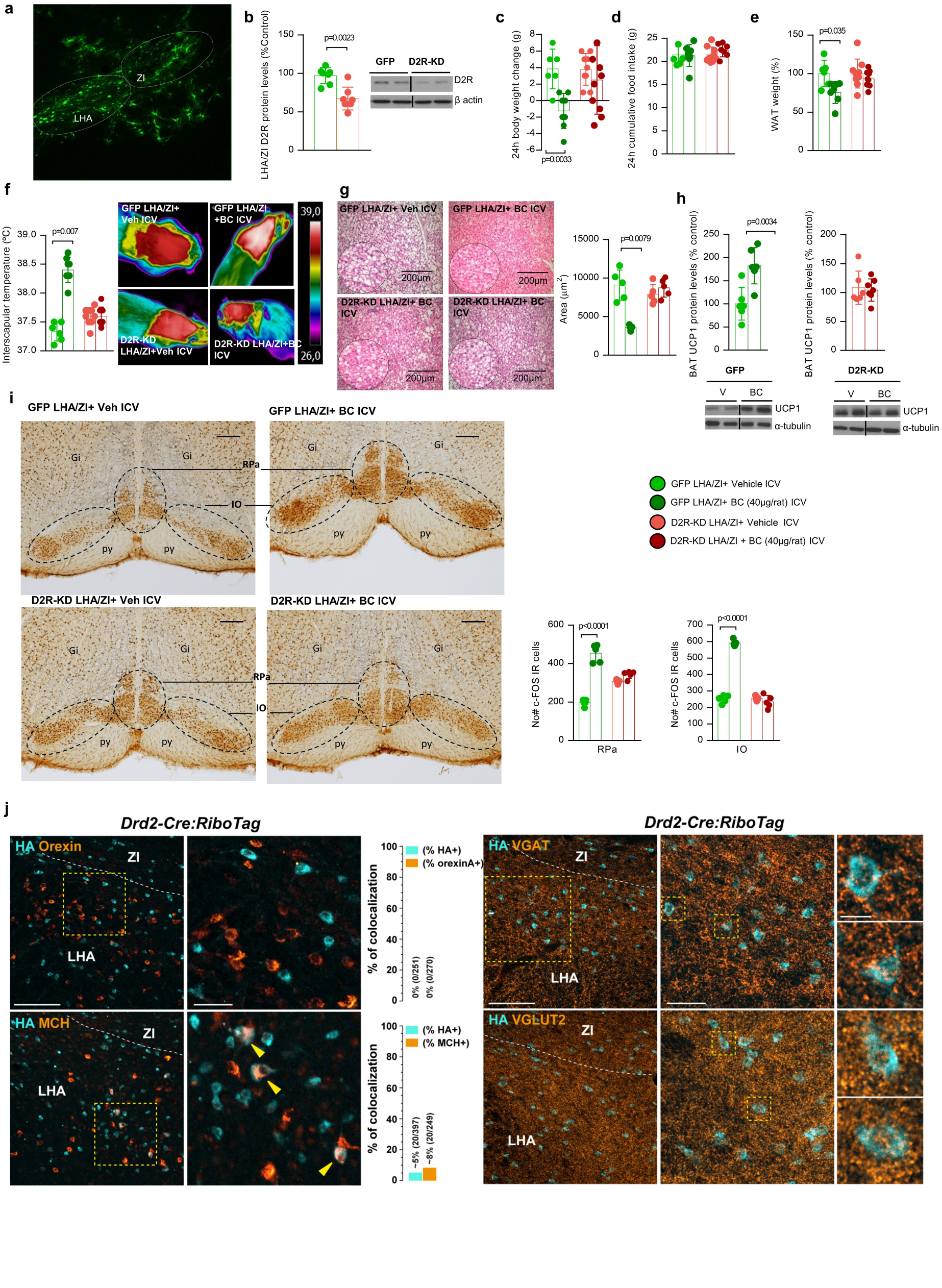
a
ZI
LHA
b
LHA/ZI D2R protein levels (%Control)
p=0.0023
GFP
D2R-KD
D2R
β actin
c
24h body weight change (g)
p=0.0033
d
24h cumulative food intake (g)
e
WAT weight (%)
p=0.035
f
Interscapular temperature (°C)
p=0.007
GFP LHA/ZI+ Veh ICV
GFP LHA/ZI +BC ICV
D2R-KD LHA/ZI+Veh ICV
D2R-KD LHA/ZI+BC ICV
39,0
26,0
g
GFP LHA/ZI+ Veh ICV
GFP LHA/ZI+ BC ICV
D2R-KD LHA/ZI+ BC ICV
D2R-KD LHA/ZI+ BC ICV
200µm
Area (µm²)
p=0.0079
h
BAT UCP1 protein levels (% control)
p=0.0034
GFP
D2R-KD
V
BC
UCP1
α-tubulin
i
GFP LHA/ZI+ Veh ICV
GFP LHA/ZI+ BC ICV
Gi
RPa
IO
py
D2R-KD LHA/ZI+ Veh ICV
D2R-KD LHA/ZI+ BC ICV
No# c-FOS IR cells
p<0.0001
RPa
IO
GFP LHA/ZI+ Vehicle ICV
GFP LHA/ZI+ BC (40µg/rat) ICV
D2R-KD LHA/ZI+ Vehicle ICV
D2R-KD LHA/ZI + BC (40µg/rat) ICV
j
Drd2-Cre:RiboTag
HA Orexin
ZI
LHA
HA MCH
% of colocalization
(% HA+)
(% orexinA+)
0% (0/251)
0% (0/270)
(% MCH+)
~5% (20/397)
~8% (20/249)
HA VGAT
HA VGLUT2

Figure 4

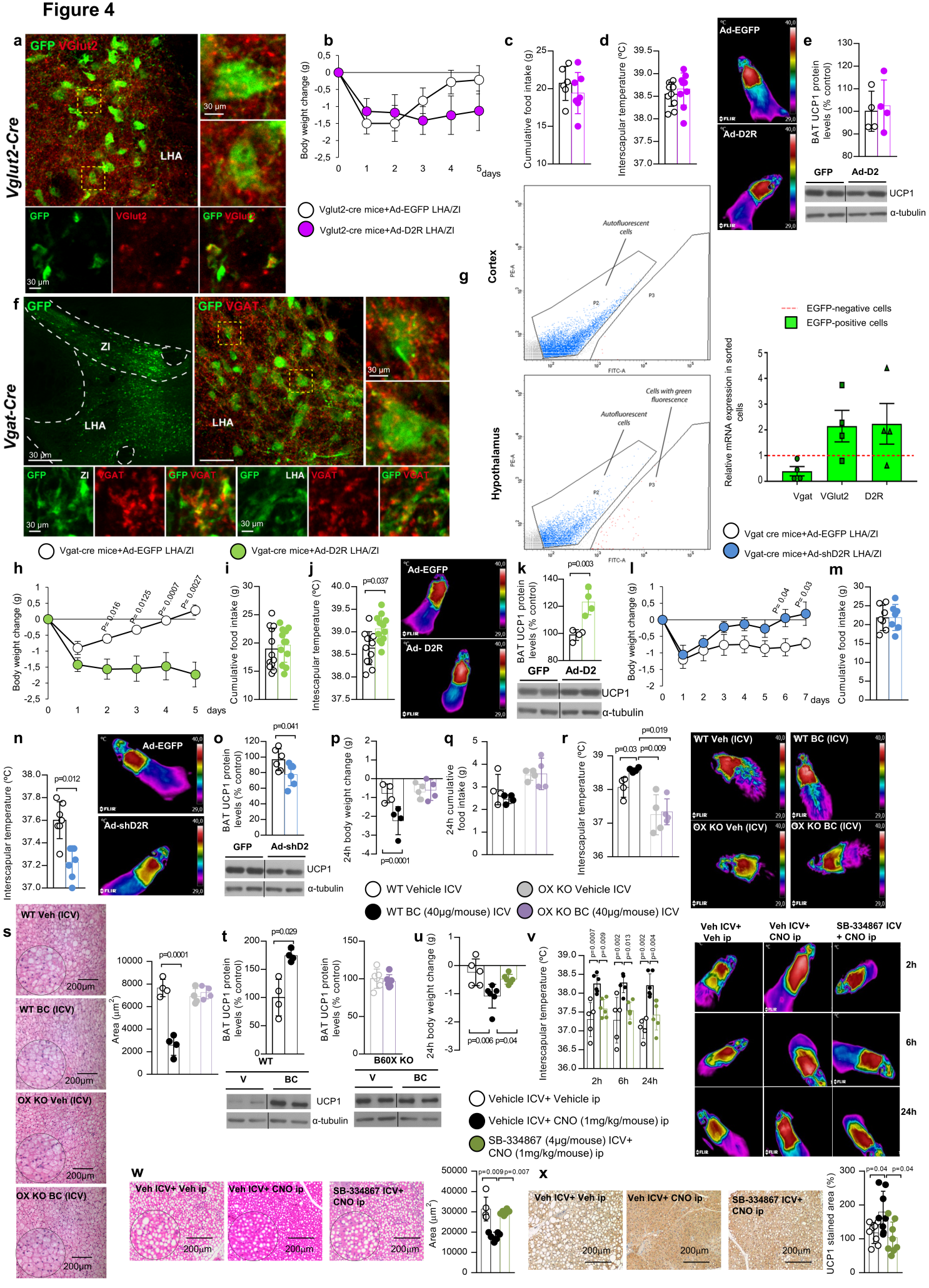
a
Vglut2-Cre
GFP VGlut2
LHA
30 µm
GFP
VGlut2
GFP VGlut2
b
Body weight change (g)
days
Vglut2-cre mice+Ad-EGFP LHA/ZI
Vglut2-cre mice+Ad-D2R LHA/ZI
c
Cumulative food intake (g)
d
Interscapular temperature (°C)
Ad-EGFP
Ad-D2R
e
BAT UCP1 protein levels (% control)
GFP
Ad-D2
UCP1
α-tubulin
f
Vgat-Cre
GFP
ZI
LHA
GFP VGAT
GFP ZI VGAT
GFP LHA VGAT
Vgat-cre mice+Ad-EGFP LHA/ZI
Vgat-cre mice+Ad-D2R LHA/ZI
g
Cortex
Hypothalamus
Autofluorescent cells
Cells with green fluorescence
P2
P3
PE-A
FITC-A
EGFP-negative cells
EGFP-positive cells
Relative mRNA expression in sorted cells
Vgat
VGlut2
D2R
Vgat cre mice+Ad-EGFP LHA/ZI
Vgat-cre mice+Ad-shD2R LHA/ZI
h
P= 0.016
P= 0.0125
P= 0.0007
P= 0.0027
i
j
p=0.037
k
p=0.003
l
P= 0.04
P= 0.03
m
n
p=0.012
o
p=0.041
Ad-shD2R
p
24h body weight change (g)
p=0.0001
q
24h cumulative food intake (g)
r
p=0.03
p=0.009
p=0.019
WT Veh (ICV)
WT BC (ICV)
OX KO Veh (ICV)
OX KO BC (ICV)
WT Vehicle ICV
WT BC (40µg/mouse) ICV
OX KO Vehicle ICV
OX KO BC (40µg/mouse) ICV
s
Area (µm²)
p=0.0001
t
p=0.029
WT
B60X KO
V
BC
u
p=0.006
p=0.04
v
p=0.0007
p=0.009
p=0.002
p=0.013
p=0.002
p=0.004
2h
6h
24h
Veh ICV+ Veh ip
Veh ICV+ CNO ip
SB-334867 ICV + CNO ip
Vehicle ICV+ Vehicle ip
Vehicle ICV+ CNO (1mg/kg/mouse) ip
SB-334867 (4µg/mouse) ICV+ CNO (1mg/kg/mouse) ip
w
SB-334867 ICV+ CNO ip
p=0.009
p=0.007
x
UCP1 stained area (%)
p=0.04
200µm

Figure 5

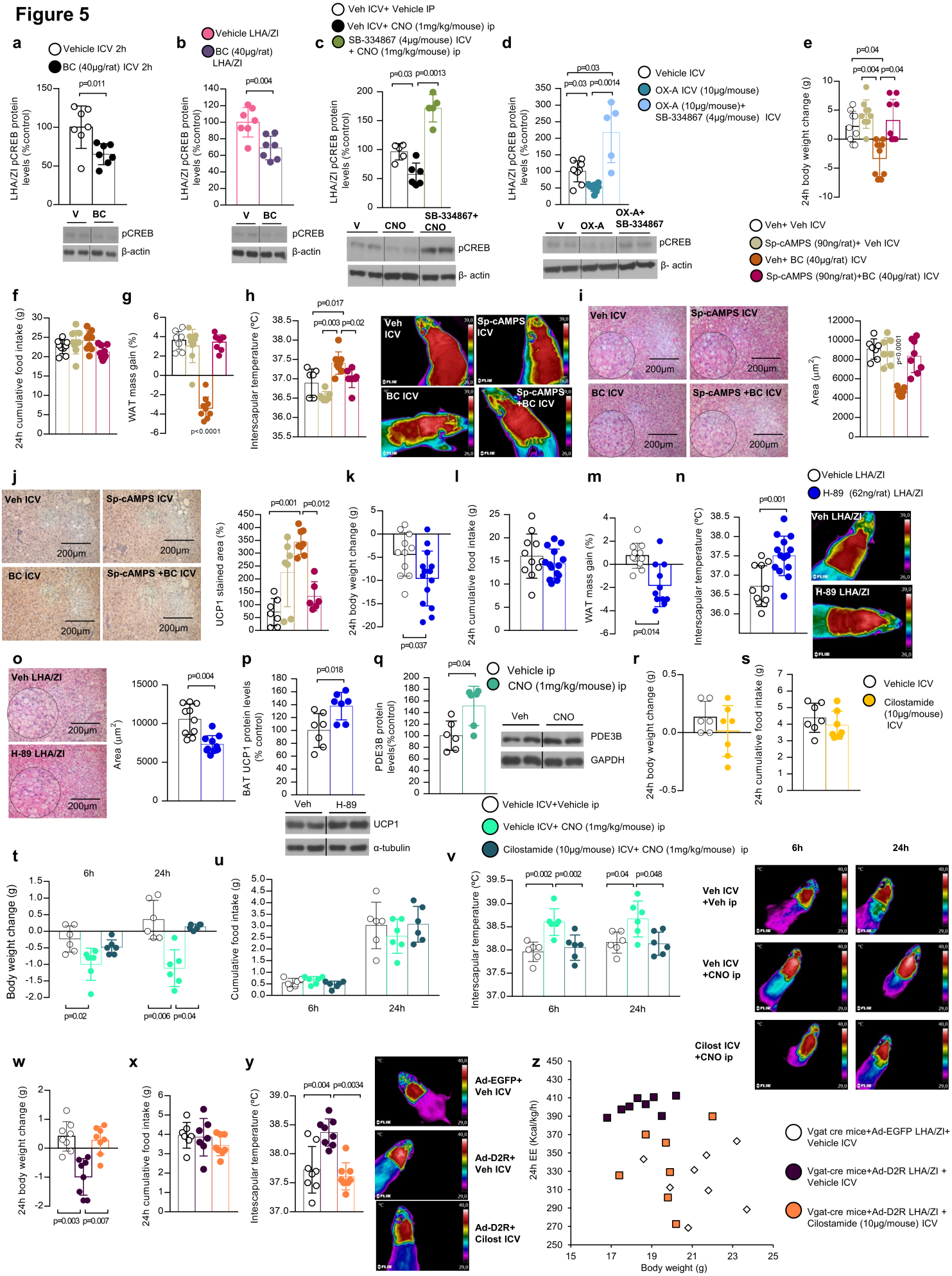
a
Vehicle ICV 2h
BC (40µg/rat) ICV 2h
LHA/ZI pCREB protein levels (%control)
p=0.011
V
BC
pCREB
β-actin
b
Vehicle LHA/ZI
BC (40µg/rat) LHA/ZI
p=0.004
c
Veh ICV+ Vehicle IP
Veh ICV+ CNO (1mg/kg/mouse) ip
SB-334867 (4µg/mouse) ICV + CNO (1mg/kg/mouse) ip
p=0.03 p=0.0013
SB-334867+ CNO
d
p=0.03
p=0.03 p=0.0014
Vehicle ICV
OX-A ICV (10µg/mouse)
OX-A (10µg/mouse)+ SB-334867 (4µg/mouse) ICV
OX-A+ SB-334867
β- actin
e
p=0.04
p=0.004 p=0.04
24h body weight change (g)
Veh+ Veh ICV
Sp-cAMPS (90ng/rat)+ Veh ICV
Veh+ BC (40µg/rat) ICV
Sp-cAMPS (90ng/rat)+BC (40µg/rat) ICV
f
24h cumulative food intake (g)
g
WAT mass gain (%)
p<0.0001
h
Interscapular temperature (ºC)
p=0.017
p=0.003 p=0.02
Veh ICV
Sp-cAMPS ICV
BC ICV
Sp-cAMPS +BC ICV
i
Veh ICV
Sp-cAMPS ICV
BC ICV
Sp-cAMPS +BC ICV
200µm
Area (µm2)
p<0.0001
j
Veh ICV
Sp-cAMPS ICV
BC ICV
Sp-cAMPS +BC ICV
200µm
UCP1 stained area (%)
p=0.001 p=0.012
k
24h body weight change (g)
p=0.037
l
24h cumulative food intake (g)
m
WAT mass gain (%)
p=0.014
n
Interscapular temperature (ºC)
p=0.001
Vehicle LHA/ZI
H-89 (62ng/rat) LHA/ZI
Veh LHA/ZI
H-89 LHA/ZI
o
Veh LHA/ZI
H-89 LHA/ZI
200µm
Area (µm2)
p=0.004
p
BAT UCP1 protein levels (% control)
p=0.018
Veh
H-89
UCP1
α-tubulin
q
PDE3B protein levels(%control)
p=0.04
Vehicle ip
CNO (1mg/kg/mouse) ip
Veh
CNO
PDE3B
GAPDH
r
24h body weight change (g)
s
24h cumulative food intake (g)
Vehicle ICV
Cilostamide (10µg/mouse) ICV
Vehicle ICV+Vehicle ip
Vehicle ICV+ CNO (1mg/kg/mouse) ip
Cilostamide (10µg/mouse) ICV+ CNO (1mg/kg/mouse) ip
t
6h
24h
Body weight change (g)
p=0.02
p=0.006 p=0.04
u
Cumulative food intake (g)
6h
24h
v
Interscapular temperature (ºC)
p=0.002 p=0.002
p=0.04 p=0.048
6h
24h
6h
24h
Veh ICV +Veh ip
Veh ICV +CNO ip
Cilost ICV +CNO ip
w
24h body weight change (g)
p=0.003 p=0.007
x
24h cumulative food intake (g)
y
Intescapular temperature (ºC)
p=0.004 p=0.0034
Ad-EGFP+ Veh ICV
Ad-D2R+ Veh ICV
Ad-D2R+ Cilost ICV
z
24h EE (Kcal/kg/h)
Body weight (g)
Vgat cre mice+Ad-EGFP LHA/ZI+ Vehicle ICV
Vgat-cre mice+Ad-D2R LHA/ZI + Vehicle ICV
Vgat-cre mice+Ad-D2R LHA/ZI + Cilostamide (10µg/mouse) ICV

Figure 6

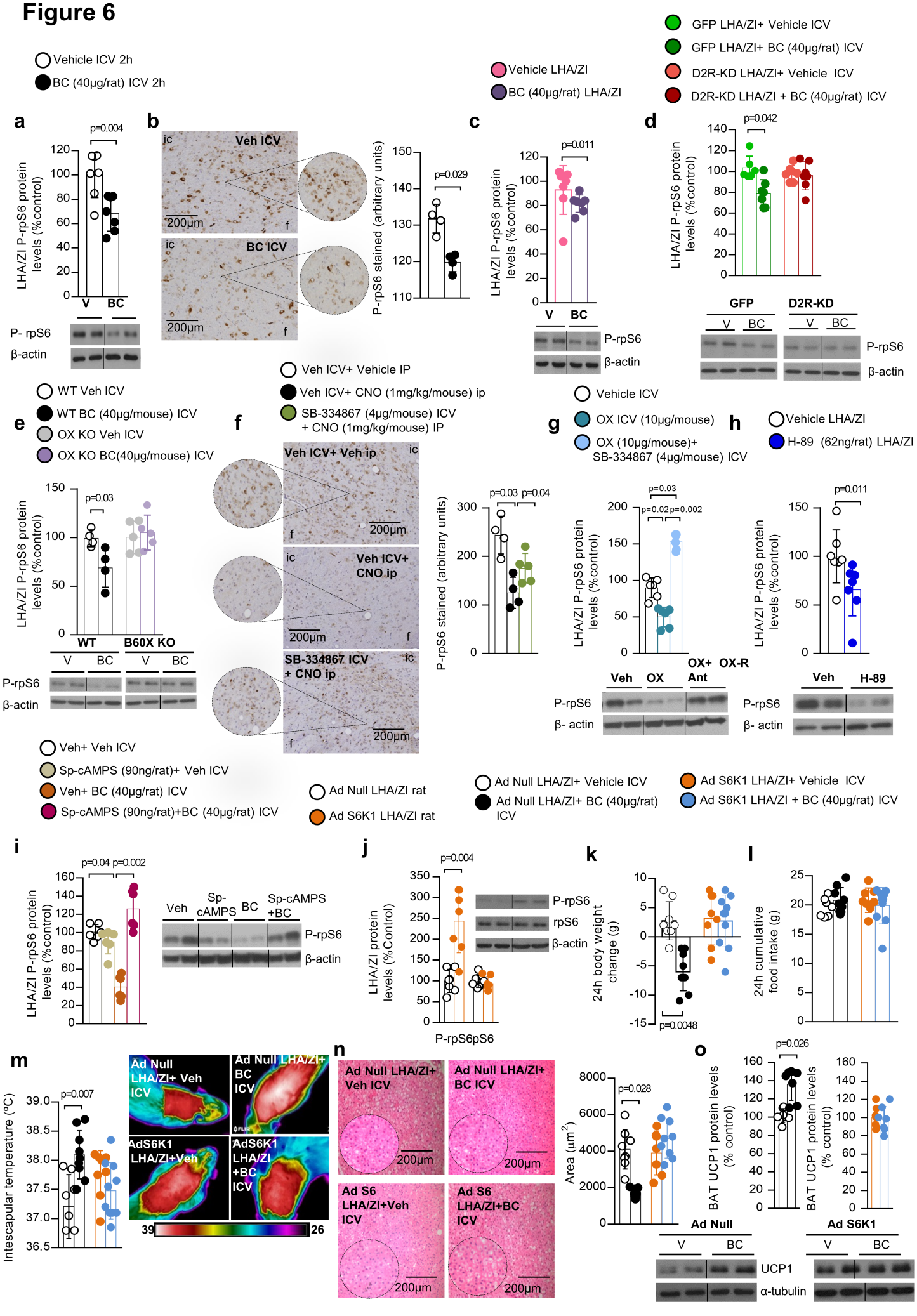
Vehicle ICV 2h
BC (40µg/rat) ICV 2h
Vehicle LHA/ZI
BC (40µg/rat) LHA/ZI
GFP LHA/ZI+ Vehicle ICV
GFP LHA/ZI+ BC (40µg/rat) ICV
D2R-KD LHA/ZI+ Vehicle ICV
D2R-KD LHA/ZI + BC (40µg/rat) ICV
a
b
c
d
LHA/ZI P-rpS6 protein levels (%control)
P-rpS6 stained (arbitrary units)
p=0.004
p=0.029
p=0.011
p=0.042
V
BC
GFP
D2R-KD
P- rpS6
P-rpS6
β-actin
Veh ICV
BC ICV
200µm
WT Veh ICV
WT BC (40µg/mouse) ICV
OX KO Veh ICV
OX KO BC(40µg/mouse) ICV
Veh ICV+ Vehicle IP
Veh ICV+ CNO (1mg/kg/mouse) ip
SB-334867 (4µg/mouse) ICV
+ CNO (1mg/kg/mouse) IP
Vehicle ICV
OX ICV (10µg/mouse)
OX (10µg/mouse)+
SB-334867 (4µg/mouse) ICV
Vehicle LHA/ZI
H-89 (62ng/rat) LHA/ZI
e
f
g
h
p=0.03
WT
B60X KO
Veh ICV+ Veh ip
Veh ICV+
CNO ip
SB-334867 ICV
+ CNO ip
p=0.03 p=0.04
p=0.02 p=0.002
OX+ Ant
OX-R
Veh
OX
H-89
β- actin
Veh+ Veh ICV
Sp-cAMPS (90ng/rat)+ Veh ICV
Veh+ BC (40µg/rat) ICV
Sp-cAMPS (90ng/rat)+BC (40µg/rat) ICV
Ad Null LHA/ZI rat
Ad S6K1 LHA/ZI rat
Ad Null LHA/ZI+ Vehicle ICV
Ad Null LHA/ZI+ BC (40µg/rat) ICV
Ad S6K1 LHA/ZI+ Vehicle ICV
Ad S6K1 LHA/ZI + BC (40µg/rat) ICV
i
j
k
l
p=0.04 p=0.002
Sp-cAMPS
BC
Sp-cAMPS +BC
p=0.004
rpS6
LHA/ZI protein levels (%Control)
P-rpS6pS6
24h body weight change (g)
p=0.0048
24h cumulative food intake (g)
m
n
o
Intescapular temperature (°C)
p=0.007
Ad Null LHA/ZI+ Veh ICV
Ad Null LHA/ZI+ BC ICV
AdS6K1 LHA/ZI+Veh
AdS6K1 LHA/ZI +BC ICV
39
26
Ad S6 LHA/ZI+Veh ICV
Ad S6 LHA/ZI+BC ICV
Area (µm²)
p=0.028
BAT UCP1 protein levels (% control)
p=0.026
Ad Null
Ad S6K1
UCP1
α-tubulin

Figure 7

a

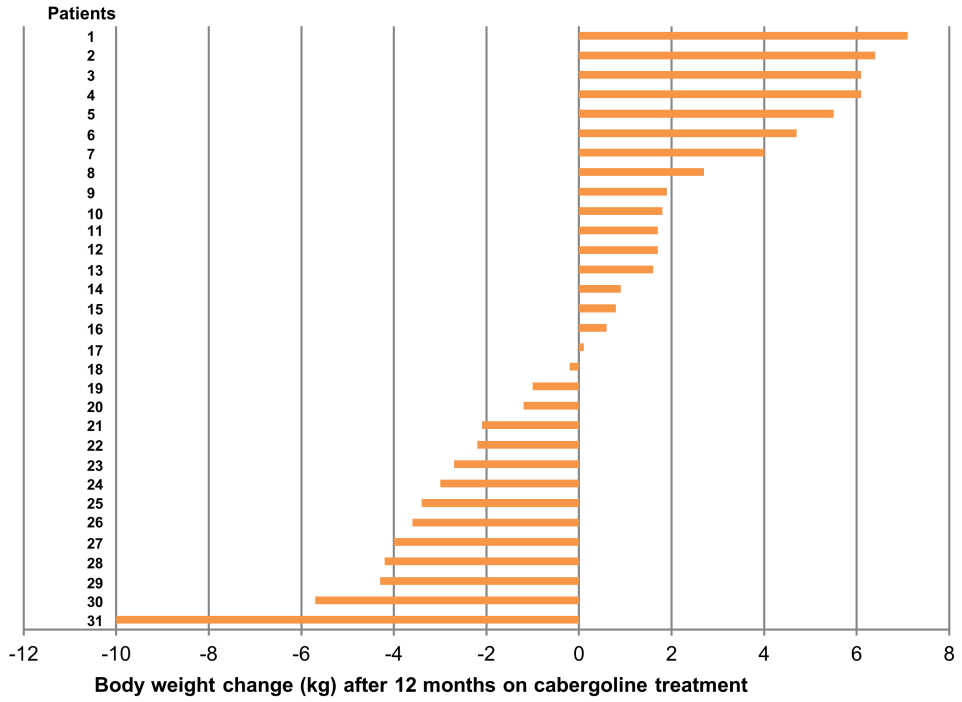

b

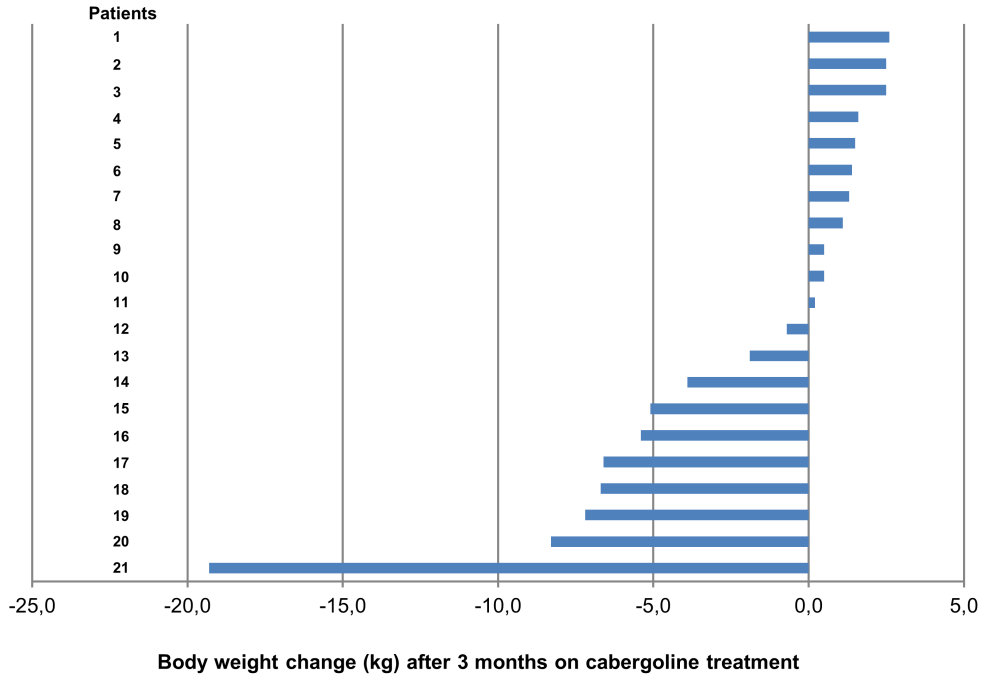

c

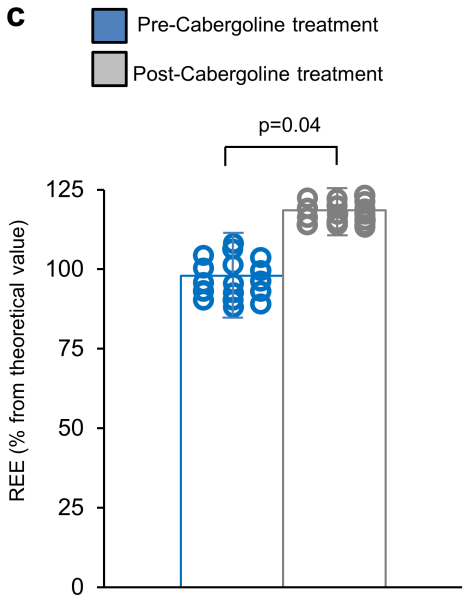

d